Controllable Needle-Free Injection
Development and Verification of a Novel Device

by

Dawn M. Wendell

B.S., Mechanical Engineering
B.S., Biology
Massachusetts Institute of Technology, 2004

Submitted to the Department of Mechanical Engineering in
Partial Fulfillment of the Requirements for the Degree of

Master of Science in Mechanical Engineering

at the

Massachusetts Institute of Technology

May 2006

Signature of Author.....
Department of Mechanical Engineering
May 5, 2006

Certified by.....
Ian W. Hunter
Hatsopoulos Professor of Mechanical Engineering
Thesis Supervisor

Accepted by.....
Lallit Anand
Professor of Mechanical Engineering
Chairman, Department Committee on Graduate Students

Controllable Needle-Free Injection
Development and Verification of a Novel Device

by

Dawn M. Wendell

Submitted to the Department of Mechanical Engineering
on May 5, 2006 in Partial Fulfillment of the Requirements for the
Degree of Master of Science in Mechanical Engineering

ABSTRACT

Current needle-free injection technology is based on actuation via compressed springs or gas. These devices are not easy to modify for different depths of injections. This thesis describes the design and verification of a handheld needle-free device which is capable of various injection depths via electrical control of a Lorentz-force voice coil actuator. A benchtop proof-of-concept device was created to prove the concept of needle-free injection using a voice coil. After the successful testing of the proof-of-concept device, a handheld prototype was designed, manufactured, and tested. The controllability of injections was tested on excised sheep tissue in-vitro. The handheld device was also tested in-vivo on sheep midside and was shown to give comparable injections to a needle for delivery of the drug collagenase. The controllable needle-free injection principles described in this thesis could be used in human or veterinary applications.

Thesis Supervisor: Ian W. Hunter
Title: Hatsopoulos Professor of Mechanical Engineering

For my grandfathers

Walter S. Nadolny 1916-2005
Matthew S. Wendell 1921-2006

Acknowledgements

First and foremost, I thank Professor Ian Hunter for giving me the opportunity to work in the BioInstrumentation Lab. I would not be writing this thesis and looking towards PhD research without his excellent guidance.

The members of the BioInstrumentation Lab have made my many days and nights in the lab enjoyable and I continue to learn from everyone's diverse set of knowledge and backgrounds. I thank the notable contributions to this project by Dr. Cathy Hogan, Dr. Andrew Taberner, Dr. Bryan Crane, Andrea Bruno, Nicalaus Sabourin, and Nathan Ball. I especially thank Brian Hemond for all of his work, as well as his friendship.

My family deserves much acclaim, especially my father who finally admits that I know more about some engineering concepts than he does.

And of course I thank Rob, who inspires me to follow my heart.

Table of Contents

1 Introduction

Drug delivery using needles has been standard practice since the mid-nineteenth century [12]. Needles have been used to inject a variety of drugs into the body, particularly those that need to be delivered locally like anesthetics or those that would be degraded or destroyed if taken orally. Needle injections of vaccines have been successful at eradicating diseases such as Rubella and Polio in the USA.

However, some people suffer from a phobia of needles (Trypanophobia), needle sticks are often painful, and cross-contamination of patients and healthcare providers from accidental needle stick injuries make needle injections dangerous. In fact, the majority of percutaneous injuries in health care workers are due to needles (as shown in Figure 1).

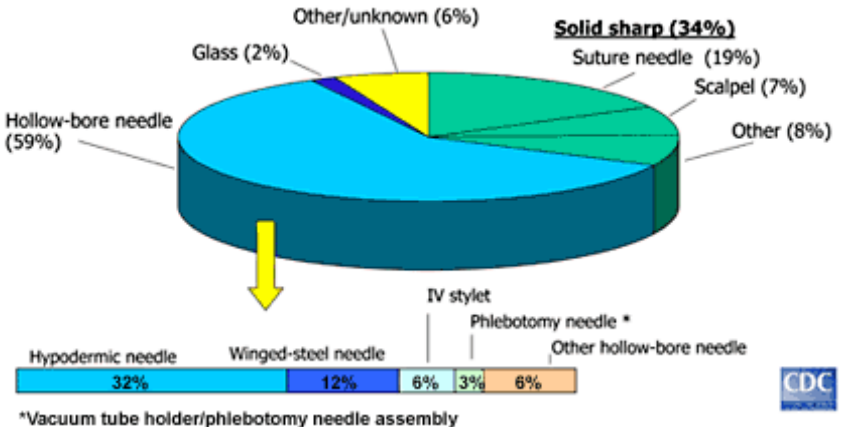

Figure 1: Devices involved in percutaneous injuries, (n=13,731 healthcare workers). Figure from the Centers for Disease Control Sharps Safety Workbook [1].

Therefore, a method of injection that does not involve needles or the pain and dangers associated with them could lead to improved healthcare across the planet.

2 Background and Motivation

2.1 Needle-Free Injection

Due to the problems that needles pose, researchers have studied other ways of drug delivery and determined that needle-free injection (NFI) was a viable alternative.

2.1.1 Historical Context

Needle-free injection was first described in the literature in 1947 as a drug delivery method that would make traditional needle injections obsolete [10]. Needle-free injection is performed by ejecting a high-pressure fluid through a small diameter nozzle into tissue. It was used beginning in the 1950s by the military for inoculations but its use was limited when researchers proved that blood-borne diseases such as Hepatitis B could be spread by the NFI devices from patient to patient [7].

2.1.2 Current Technology

Current needle-free technology used in the human market centers around single-use devices (in which the portion that is in contact with the skin is disposed after each injection). The injectors on the market are powered by compressed springs or gas [19] [18] [15] [20] [14] [17] [16] [21] [30] [24]. A common use for NFI today is insulin injection for diabetic patients. This market responds well to NFI due to the frequency of injections. The pain of frequent needle-sticks often causes a psychological aversion to needles among diabetics. NFI is good for these patients due to the lack of a needle. It is also useful for young patients, with several NFI devices being marketed especially for children. BioJect [6] developed the *cool.click* for delivering human growth hormone to pediatric patients (Figure 2a) and markets an optional set of Elephant Ears™ for use on their Biojector NFI device (Figure 2b).

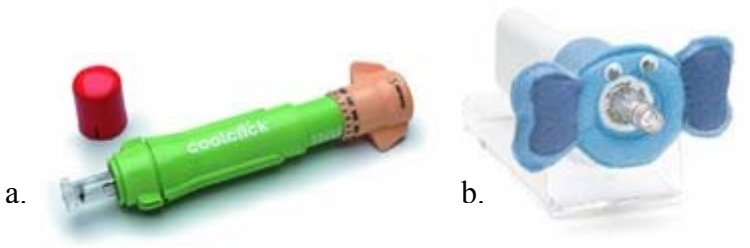

Figure 2: (a) The *cool.click* system from Bioject for injecting human growth hormone into pediatric patients and (b) optional Elephant Ears™ for use with the Biojector 2000. (Figures taken from www.bioject.com).

2.2 Animal Husbandry

Field veterinary medicine suffers from many of the same dangers associated with needles as human medicine. It is often desirable to perform many injections rapidly, and these injections may occur in a farm setting where using and disposing of needles is dangerous and inconvenient. Therefore, NFI would be an excellent solution for animal husbandry applications. Additionally, because of the frequently remote locations involved, it would be especially beneficial to have a device that was capable of many different kinds of injections with minimal changeover time.

3 Controllable NFI Project Goals

After reviewing current needle-free injection technology and applications, it became apparent that a controllable device capable of different depths of injections would be useful in both human and animal applications. With input from a sponsoring pharmaceutical company, Norwood Abbey Inc., of Victoria, Australia, we decided to design, build, and test an NFI device for the veterinary market. This device has the following functional requirements:

- Able to inject lambs
- Handheld
- Able to quickly change injection parameters
- Operates on battery power
- Automatically reloads with fluid for sequential injections
- Delivers at least 100 μL per injection
- Produces fluid injection pressures of at least 60 MPa
- Runs for at least 500 cycles without refilling with fluid or recharging the battery

In order to design a device with these constraints, we conducted an analysis of current needle-free injection theory.

4 Needle-Free Injection Theory: Mechanical Models

When needle-free injection was first described by Hingson and Hughes [10], they were not concerned with the mechanics of jet injection but instead focused on the results of successful injections. Their analysis of injection parameters was purely empirical, based on results of injections into humans and cadavers. They only specify "the fact that extremely fine high pressure jets are capable of piercing the human skin," [10] and dedicate the rest of their paper to results of patient testing. Subsequent research in this area has focused on understanding the effects of needle-free injection parameters through modeling injections into synthetic skins.

4.1 Polyacrylamide Testing

Polyacrylamide gels is often used to simulate tissue. Most recently, Schramm-Baxter and Mitragotri used polyacrylamide gels to investigate the properties of a commercially-available NFI device [25]. They hypothesized that needle-free injection occurs in two phases: creation of a central hole, and the spreading of the fluid as if it originated from a point source at the bottom of the hole. (Figure 3).

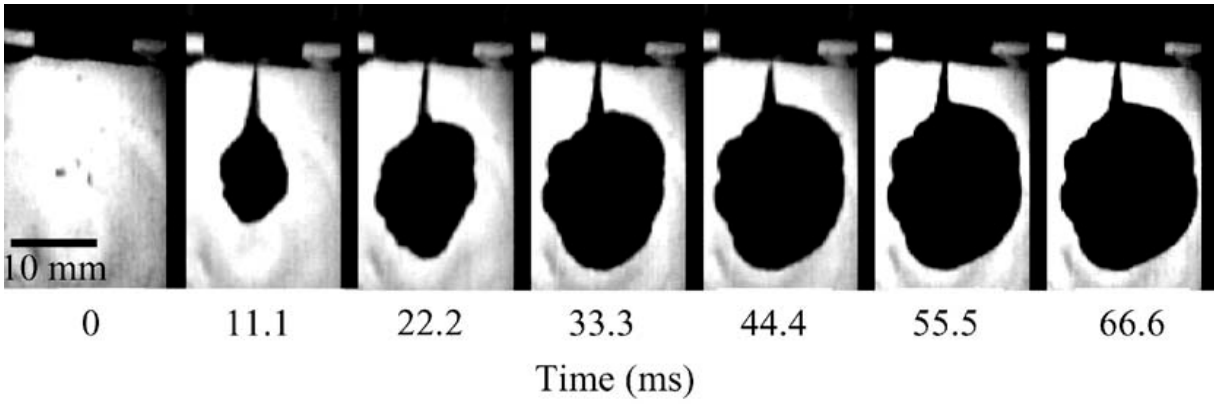

Figure 3: "The evolution of jet penetration during the injection into 20% acrylamide gel (orifice diameter 152 μm, velocity of 180 m/s, volume of 0.076 ml). The presence of an introductory channel and fluid dispersion is already evident by 11.1 ms. The jet enters the gel at the black/white interface." Figure and text from [25].

Use of polyacrylamide gel as a tissue model is limited because of its homogeneity; the polyacrylamide gel does not adequately represent the different layers of tissue near the surface of the skin. Also, the gel has a tendency to fracture along planes or crack (as visible in Figure 4 from [25]), which is not representative of tissue behavior.

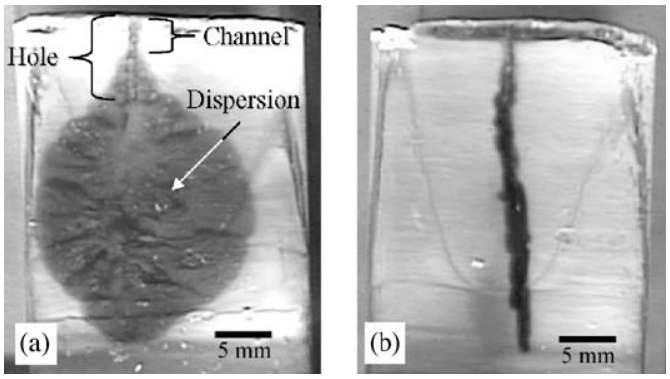

Figure 4: "A polyacrylamide gel containing 20% acrylamide was jet injected from 1mm above the top of the gel at 170 m/s with 0.076 ml of fluid of which the majority penetrated into the gel (152 mm diameter nozzle). (a) The general shape of the jet penetration into the gel has an introductory channel followed by a circular dispersion. A hole is present in the gel within the introductory channel. (b) Side view of the same gel shown in part (a). The figure shows dispersion of the jet in the gel is two dimensional." Figure and text from [25].

4.2 Model Of NFI Parameters For Injections Into Tissue

The research conducted by Schramm-Baxter and Mitragotri also described injections into tissue using needle-free injection. They proposed a model that postulates that the depth of the injection is a function of the power of the fluid jet when it exits the device nozzle [25] [27]. Using conservation of energy of the fluid at the nozzle and assuming a flat velocity profile in the fluid, the power at the nozzle is

$$P_n = \frac{1}{2}\dot{m}\,u_n^2, \tag{1}$$

where P_n is the jet power at the nozzle, $\dot{m}$ is the mass flow rate through the nozzle, and u_n is the fluid velocity at the nozzle. The mass flow rate is defined as

$$\dot{m} = \rho A_n u_n, \tag{2}$$

where ρ is the density of the fluid and the area of the nozzle is A_n. The area of the nozzle in terms of the diameter is

$$A_n = \frac{\pi D_n^2}{4}. \tag{3}$$

Therefore, the jet power at the nozzle in terms of the fluid density, nozzle diameter, and fluid velocity at the nozzle is

$$P_n = \frac{\pi}{8}\rho D_n^2 u_n^3. \tag{4}$$

However, it is extremely difficult to measure the fluid velocity at the nozzle. Therefore, we conducted experiments to find a model that could approximate the fluid velocity from other parameters that are easier to measure. In our model, we determined the velocity from the pressure of the fluid in the cylinder using the Bernoulli Equation, giving

$$u_n = \sqrt{2\rho p}\,, \tag{5}$$

where p is the pressure of the fluid that is being injected. Combining Equations 4 and 5, the jet power in terms of the fluid density, nozzle diameter, and pressure is

$$P_n = \frac{\pi}{\sqrt{8}} \rho^{5/2} D_n^2 p^{3/2}. \tag{6}$$

The Bernoulli Equation involves several simplifications, including steady inviscid flow, constant fluid density, and no heat or work transfer through the fluid. At first, it appears that the NFI fluid flow may not meet these criteria. Experiments were performed to see if the Bernoulli Equation could predict reasonable fluid velocities. The pressure in the fluid during the injection was measured every 100 μs. For each pressure data point, the mass flow rate was calculated by combining Equations 2 and 5:

$$\dot{m} = \rho^{3/2} A_n \sqrt{2p}\,. \tag{7}$$

Integrating the calculated mass flow during the time of the injection yielded a theoretical volume of fluid ejected which was then compared to the measured volume of fluid ejected through the nozzle. (See Matlab [21] program written for calculating jet power and integrating volume of fluid ejected in Appendix B.) The Bernoulli estimate was compared with estimates from models that took into account possible viscous losses, turbulence, or entry regions. However, the Bernoulli model best predicted the measured volume ejected by the device, and the model described by Equation 6 was used as the working model during the duration of the project.

An important improvement in our model over the Schramm-Baxter model of jet injection was our calculation of the jet power at every sampled data-point. Schramm-Baxter only used the average jet pressure over the entire injection to calculate jet power [25] [27]. However, due to the controllability of this NFI device, we needed to measure and understand the jet power throughout the course of the injection.

5 Benchtop Proof of Concept

To demonstrate the feasibility of an electrically-controllable NFI device, a benchtop proof-of-concept device was developed first. A voice coil was selected as the controllable actuator so that the pressure of the fluid could be varied during the injection, thus varying the jet power during the injection. A functional diagram of the device is shown below (Figure 5).

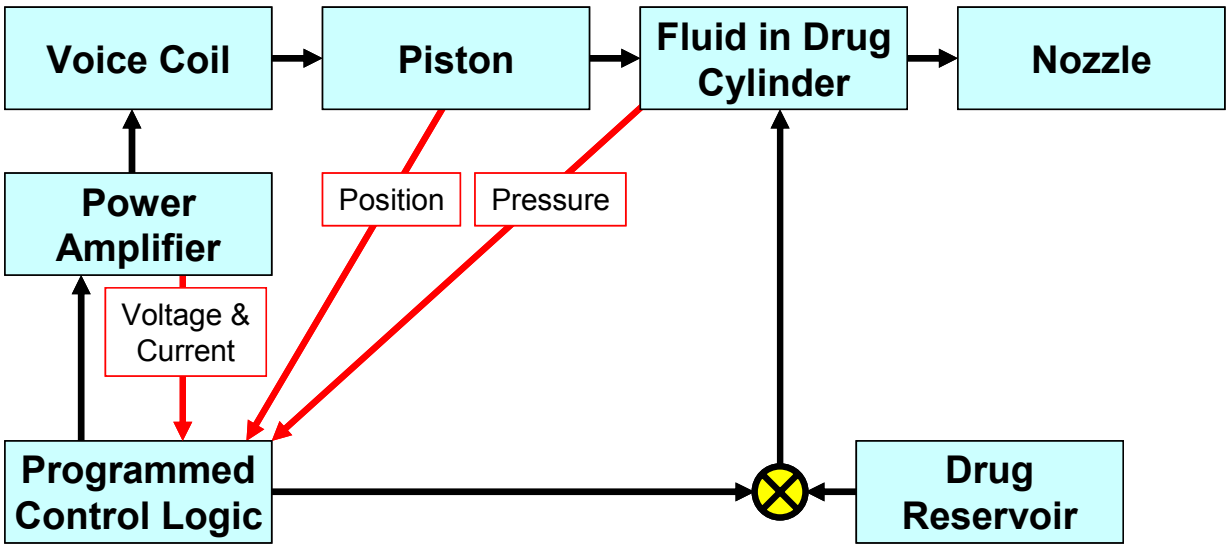

Figure 5: Functional Diagram of the controllable needle-free injector. The path of action is shown with black arrows. Sensor feedback is shown by red arrows.

5.1 Device Design

The benchtop device was oriented vertically, so that the sample could be simply placed underneath. The components were aligned axially and mounted using Macrobench components [21]. Figure 6 shows a model of the device and the actual implementation.

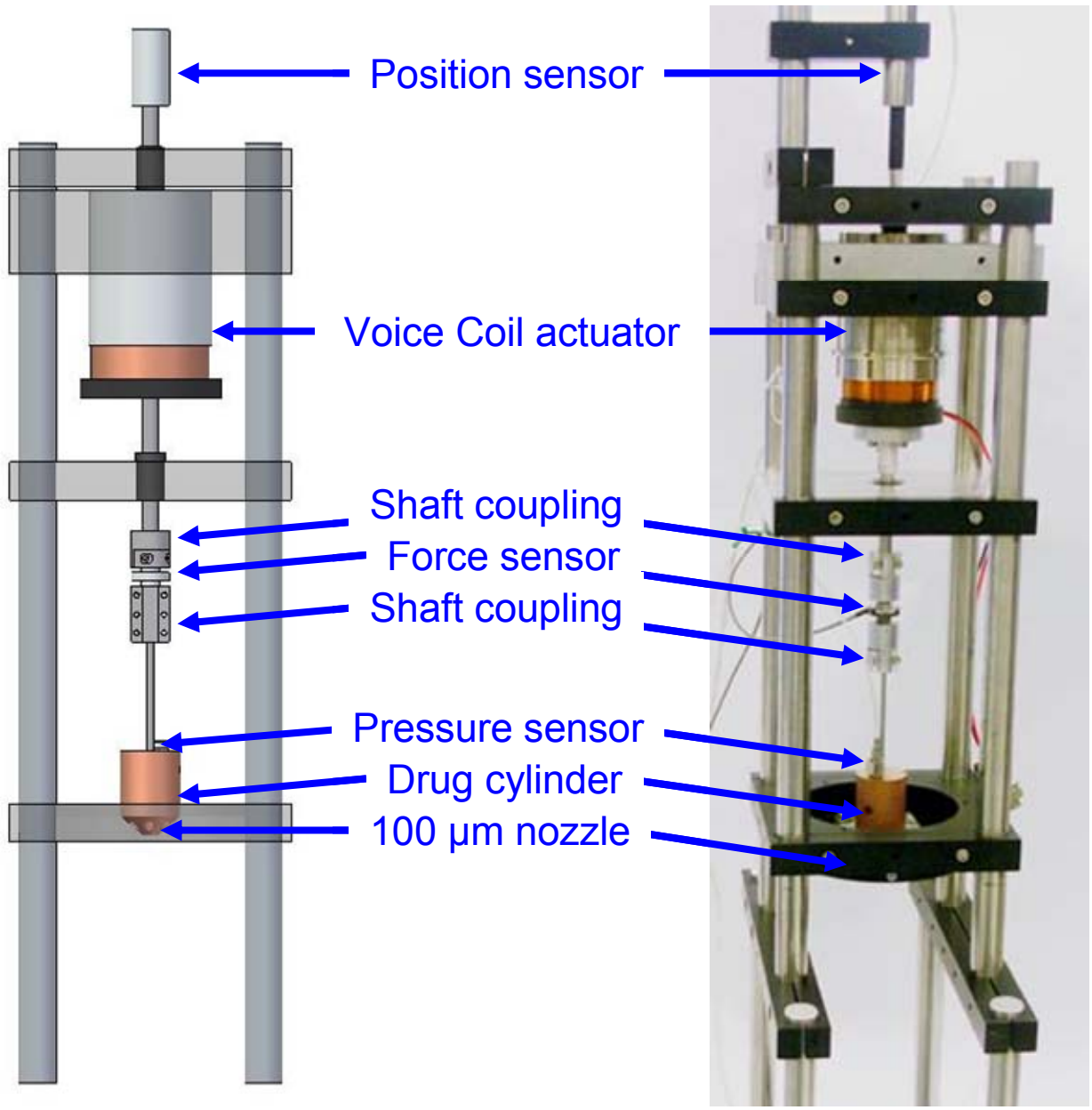

Figure 6: Benchtop proof-of-concept controllable needle-free injection device. The CAD drawing is on the left and the actual device is on the right.

5.1.1 Voice Coil

A commercially-available voice coil (BEI Kimco Magnetics [5] model LA25-42-000A) was selected for use in the device. The coil is rated for 266 N of continuous stall force, with a DC resistance of 2.4 Ω and a force constant of 21 N/A. The total stroke is 25.4 mm. The force output as a function of position was determined by labmate Nathan Ball, as shown in Figure 7.

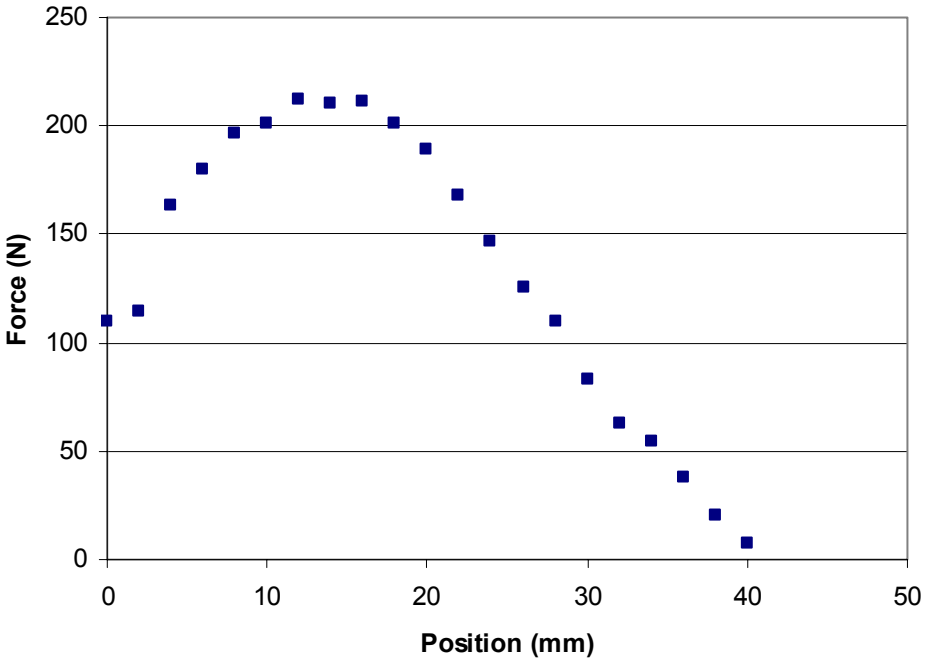

Figure 7: Plot of force available from voice coil as a function of its position at 10 Amperes. Experiment and analysis performed by Nathan Ball.

The magnetic properties of the coil were also modeled in ANSYS 8.1 [3] by Dr. Andrew Taberner (Figure 8). This modeling was used to confirm that the selected voice coil was capable of the required force. Also, an understanding of the magnetic field in the voice coil would be important to Dr. Taberner's ongoing project to design and build an optimum voice coil for this application.

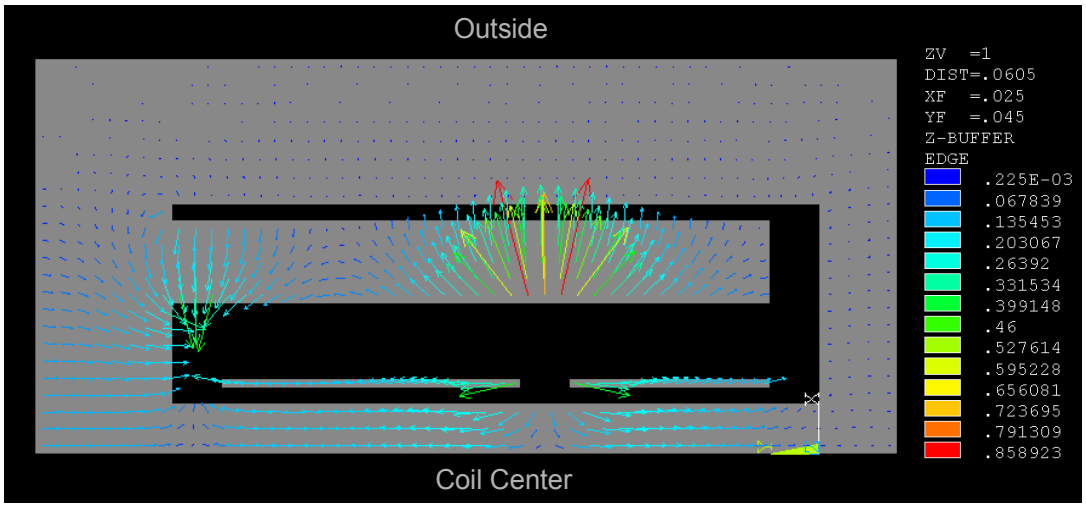

Figure 8: ANSYS 8.1 model of the magnetic field in the BEI Kimco model LA25-42-000A voice coil. Note the non-uniformity of the field, which corresponds to the varying force over displacement shown in Figure 7. (Modeling and figure courtesy of Dr. Andrew Taberner).

5.1.2 Piston Assembly

Connecting the voice coil to the rest of the system was a central shaft, also called the piston assembly. A 6.35 mm shaft was attached to the coil of the voice coil actuator and extended up to the position sensor and down to a coupler that linked to a force sensor. Below the force sensor there was a 3 mm shaft ("the piston") that fit tightly into the drug cylinder.

5.1.3 Drug Cylinder and Nozzle

The drug cylinder was designed to hold the fluid to be injected, interface with the nozzle, piston, and pressure sensor, and allow for filling and refilling with minimal trapped air. Therefore, the drug cylinder (Figure 9) was a complicated element designed and machined primarily by Brian Hemond, a graduate student in the BioInstrumentation Laboratory.

The 3 mm piston entered the drug cylinder at the central bore (at the top of the figure). The central bore was filled with fluid by the refill port on the right side. A ball check valve allowed fluid to enter the system via the refill port but prevented the fluid from back-flowing when the device was fired. On the left side of the drug cylinder, there were bores for a pressure sensor (described in Section 5.1.4) and a bleed port; the bleed port was opened during the initial filling of the system to allow trapped air to escape. At the bottom of the drug cylinder was the nozzle. The nozzle was a separate component that had a central bore aligned with the drug cylinder central bore and an orifice at its end. The orifice was 100 μm in diameter and created by microdrilling the end of the nozzle.

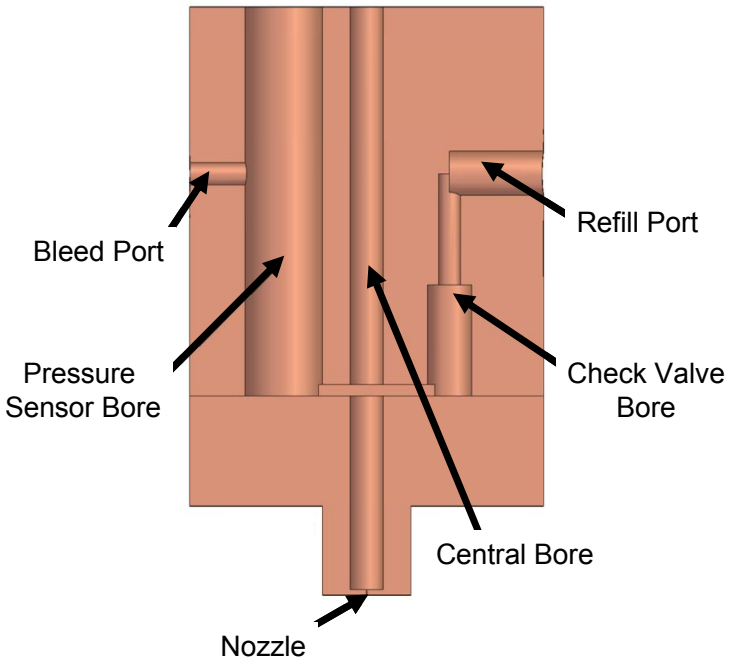

Figure 9: Cross-section of benchtop prototype drug cylinder, designed by Brian Hemond.

5.1.4 Sensors

The benchtop proof-of-concept device was equipped with 3 sensors: position, pressure, and force. The position sensor (DC Fastar DCFS3/4-M LVDT [29]) was mounted at the top of the device and measured the position of the piston assembly. The piezoelectric pressure sensor (Kistler type 211B1 [12]) was mounted in the drug cylinder and measured the pressure of the fluid in the cylinder. The force sensor (Futek 250-lb load cell [8]) was included in the design to measure the force needed for injection. This data would be used to determine the specifications of the actuator for future devices.

5.1.5 Electronics and Software

The electronics for the system and the control software were the Master of Engineering thesis project of Brian Hemond. (For a more in-depth discussion of the electrical side of this project, please see his thesis [10]). The voice coil was powered by a linear amplifier (AE Techron [2] LVC 5050) under the control of the system's programmed control logic (PCL) written by Brian Hemond. The PCL sent a voltage signal ("waveform") to the amplifier that then amplified it and sent it to the voice coil. The PCL also recorded the sensor outputs. The user interface (Figure 10) filtered and displayed the sensor signals, as well as the voltage and current sent to the coil during the injection.

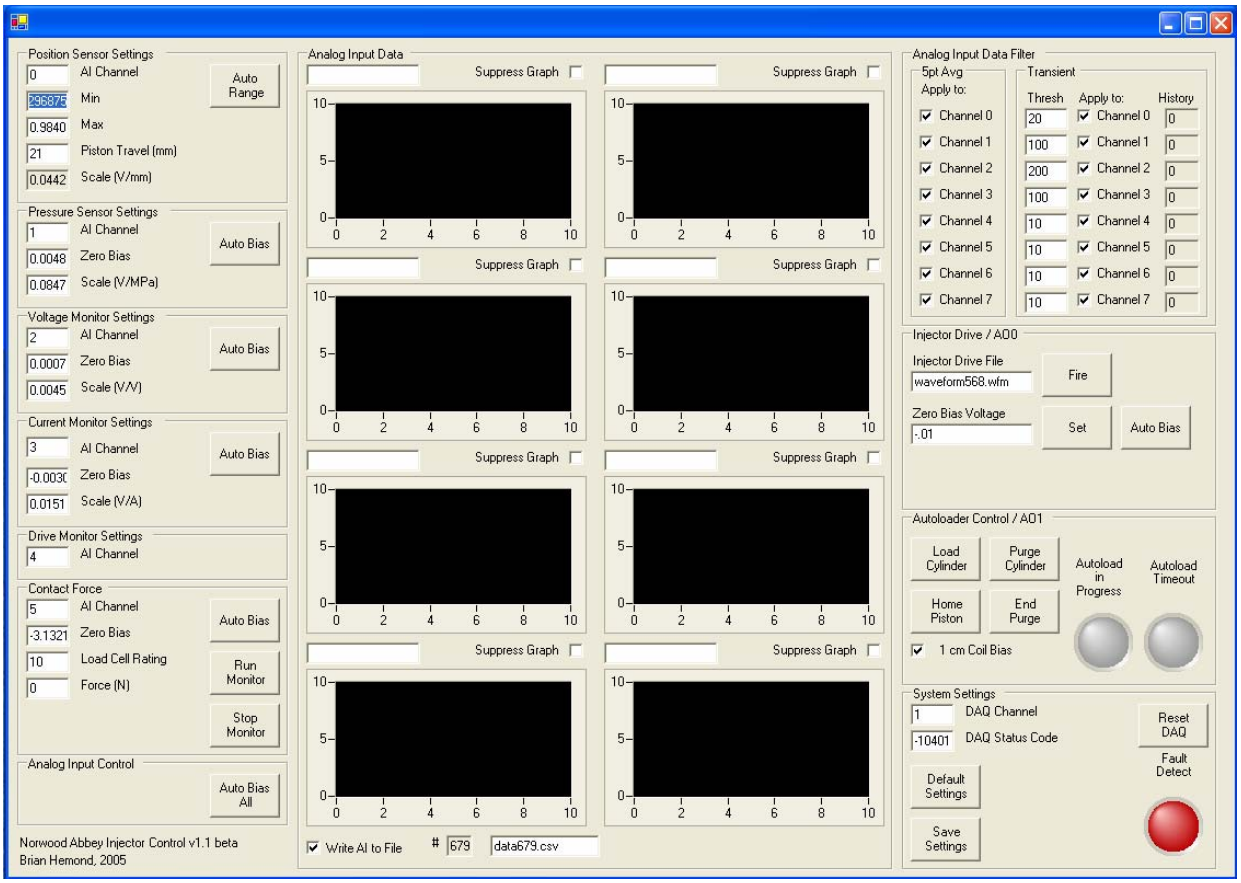

Figure 10: The user interface of the programmed control logic. Each of the black panels displays plots of the sensor feedbacks during an injection. The software also automatically logged all data (raw and filtered) to a comma-separated-variable file.

Varying the voltage signal sent by the PCL changed the parameters of the injection. Increasing the voltage led to higher pressure in the fluid due to the increased force generated by the voice coil and transmitted to the fluid through the piston assembly. Therefore increasing the voltage resulted in higher jet power at the nozzle. Each voltage waveform corresponded to a jet power waveform whose results in tissue were then observed.

5.2 Device Characterization

The benchtop device was tested to verify that it was capable of injection.

5.2.1 Repeatability

The repeatability of the injected volume was tested before performing any biological injections. Ten injections were made using the same control parameters. The fluid ejected from the nozzle was collected in Eppendorf tubes and measured. The results are shown in Figure 11.

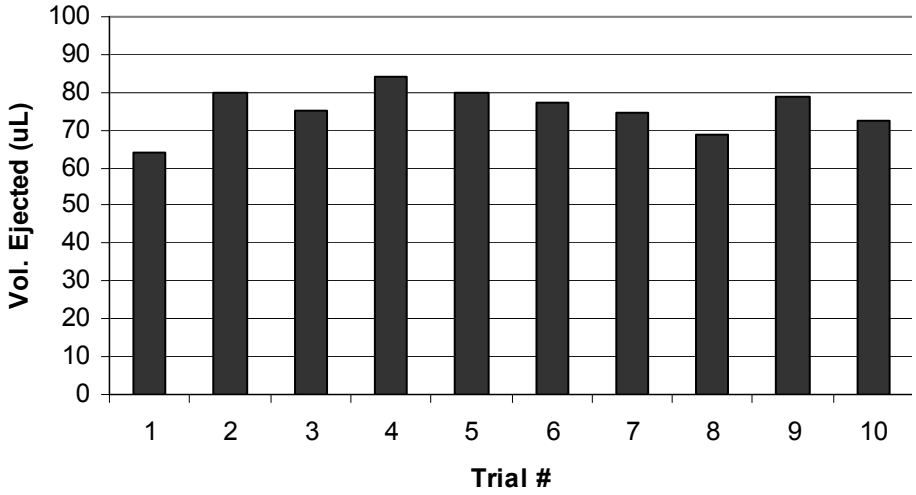

Figure 11: Volume of fluid ejected from benchtop NFI device in 10 sequential trials.

There was considerable variability between injections (standard deviation: 5.9 μL). This would be problematic in biological injections because the amount of drug injected would vary widely. The repeatability would need to be improved in the next design iteration.

5.2.2 Polyacrylamide Dye Injections

We confirmed the device was capable of injections into polyacrylamide gels and achieved results similar to Schramm-Baxter's results [25] (Figure 12).

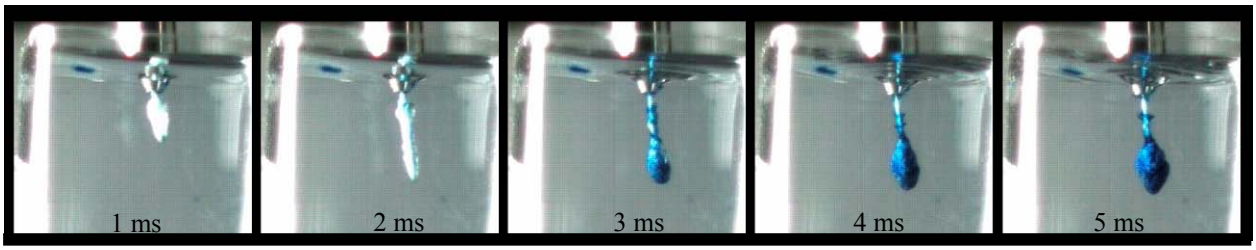

Figure 12: Sequential photographs of needle-free injection of 0.1% Bromocresol Green dye solution into polyacrylamide gel using high speed videography (Phantom V9 camera by Vision Research [31]).

5.2.3 In Vitro Dye Injections

After the polyacrylamide gel testing proved that the device was able to successfully inject fluid, testing in tissue samples was performed. Injections into postmortem skin from a 6-month old lamb showed that the device could inject into tissue (Figure 13). A 0.1% solution of the dye Bromocresol Green was injected into the tissue.

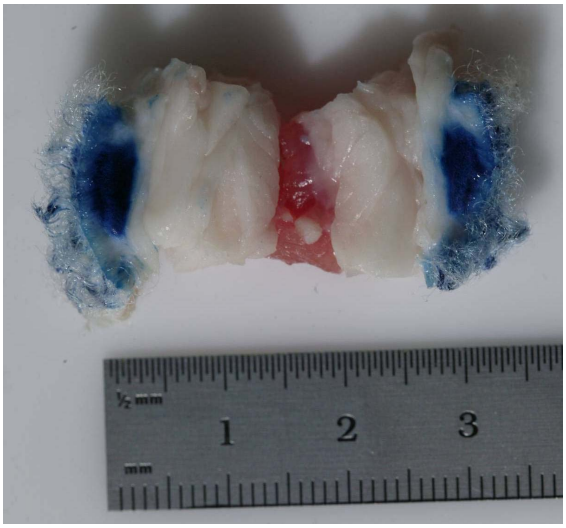

Figure 13: Tissue sample cut in half and laid open to view the injection depth from the benchtop proof-of-concept device. This injection went into the dermis of the tissue, with the majority of the fluid between 1 and 4 mm deep.

Also, in vitro testing showed that by varying the voltage waveform (and therefore the jet power waveform), different depths of injections were possible (Figure 14).

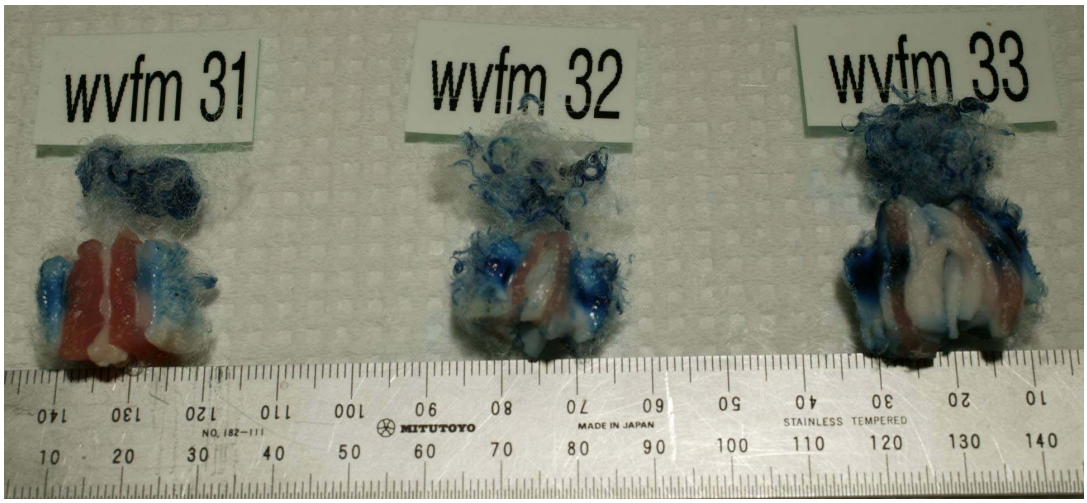

Figure 14: Tissue samples cut in half and laid open to view the injection depth from the benchtop proof-of-concept device. Each of the samples was injected using a different voltage waveform (and therefore a different jet power). The sample on the left was injected using a low jet power, the sample on the right using high jet power, and the sample in the middle using an intermediate jet power. The wool that was on each sample when it was injected has been trimmed off and placed above the sample.

5.2.4 In Vitro Activity Testing

After the success of the dye injections, it was necessary to see if the NFI system could inject an enzyme and whether that enzyme would continue to be active in the tissue. Therefore, biological activity tests were performed with the enzyme collagenase. Collagenase was chosen because assays for its activity are well-documented and its well-known pathology would make it useful for later in-vivo trials.

The experiments were performed using a biological buffer solution (1xRB) as the control and a collagenase mixture named C7926. Injections were performed into tubes and into in-vitro tissue samples. The volume of fluid was determined by measuring the mass of the samples before and after injection. The volume of fluid ejected for each sample is shown in Figure 15.

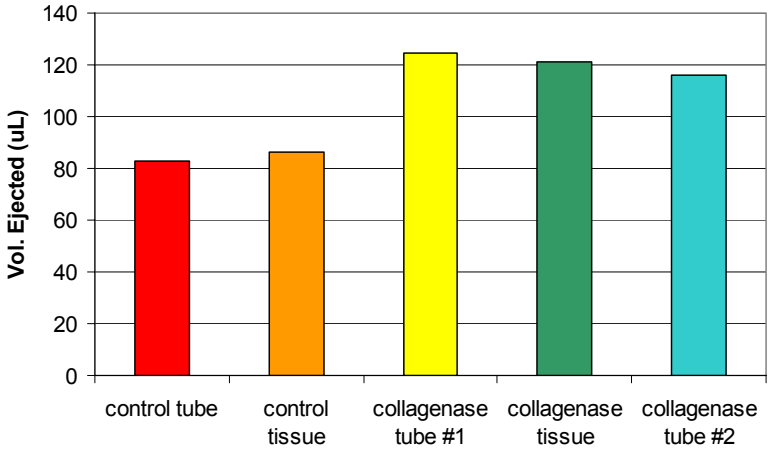

Figure 15: Volume of fluid ejected during experiments to test the activity of the enzyme collagenase after being used in the NFI Benchtop Proof of Concept.

Activity assays designed, performed, and analyzed by Dr. Cathy Hogan showed that the collagenase was still active after being ejected from the nozzle into a tube and that it was still active after being injected into tissue.

5.2.5 Summary of Results

The benchtop proof-of-concept device proved that needle-free injection can be performed using a device actuated by a voice coil. It also showed that a voice-coil-actuated NFI system could be controlled to inject to different depths. The NFI device was able to inject an enzyme into sheep tissue without causing it to denature. These results were promising enough for the project to move on to the design and manufacture of a handheld prototype device.

6 Handheld Prototype

We created a conceptual design of a handheld NFI device, shown in Figure 16.

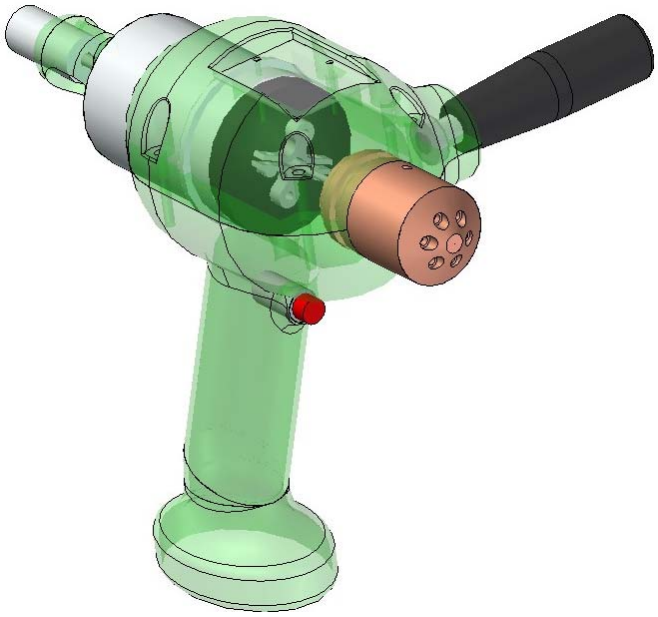

Figure 16: Conceptual design of a handheld controllable needle-free injector. The overall architecture is based on a hammer-drill design, with the possibility of a removable battery on the bottom of the handle.

A model of the device was created using stereolithography (SLA) as shown in Figure 17.

Figure 17: Rapid-prototype of conceptual design of a handheld controllable needle-free injector.

However, before moving on to such a streamlined, commercial design, the handheld prototype was designed and created with ease of manufacture and replaceable components for testing.

6.1 Device Design

The device design was changed from a vertical configuration in the benchtop device to a horizontal configuration for the handheld device. The axial alignment of the elements was achieved by an aluminum housing designed by Dr. Bryan Crane. Handles were added and several improvements over the benchtop proof-of-concept device were implemented. A cutaway CAD view and the finished device are shown in Figure 18.

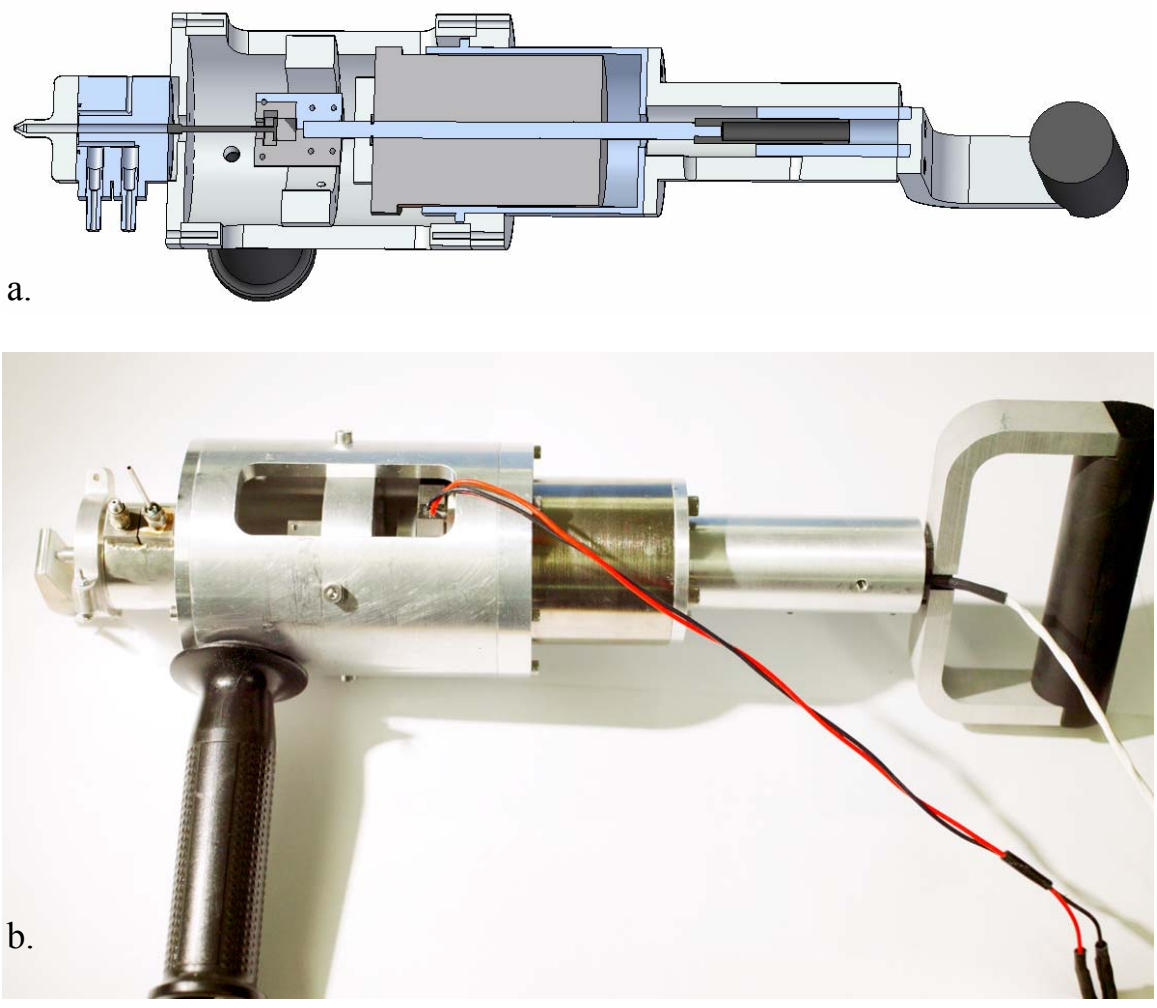

Figure 18: (a) Cutaway CAD model of the handheld NFI prototype and (b) the device (upside down so the pressure sensor and refill ports are visible).

6.1.1 Drug Cylinder

The drug cylinder design was similar to that of the benchtop device but the location of some of the fluid passageways was changed to make it easier to purge the air from the system when first

filling the device with liquid (Figure 19). Also, the cylinder was made out of stainless steel for increased corrosion resistance and biological compatibility.

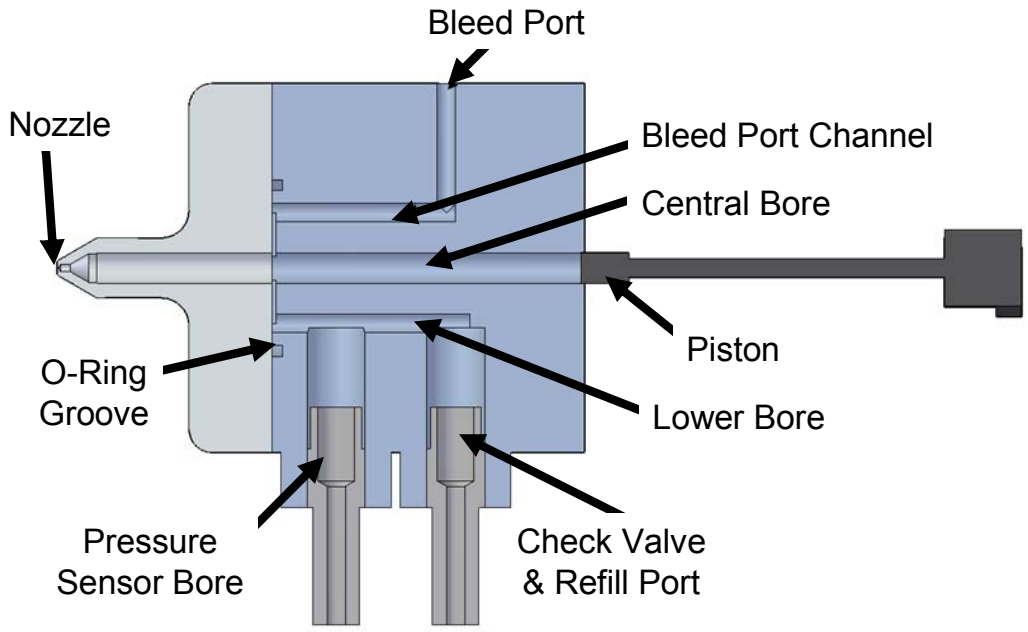

Figure 19: Cutaway CAD view of the drug cylinder and nozzle. Note the changed locations of the pressure sensor bore and bleed port channel. Also note the o-ring groove at the front of the cylinder.

Another design change from the proof-of-concept was the inclusion of an o-ring groove on the face of the cylinder (Figure 20). This o-ring prevented fluid leakage at the interface between the drug cylinder and the nozzle.

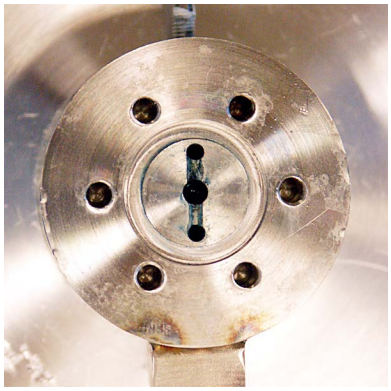

Figure 20: The face of the drug cylinder. Note the o-ring groove. The circle of holes outside of the groove are mounting holes for the nozzle.

6.1.2 Nozzle

The nozzle was redesigned for use with sheep, where wool on the samples (and on live animals) would be in the way. Labmate Nicaulas Sabourin designed the nozzle with a narrow, tapered tip

to allow the nozzle to penetrate matted wool and contact the sheep's skin (Figure 21a). He machined it using a CNC lathe [32]. A nozzle cap was designed with a bi-stable, spring-tensioned system that would seal off the nozzle so that drug was not wasted and air could not enter the system while automatically reloading (Figure 21b).

a.  b. 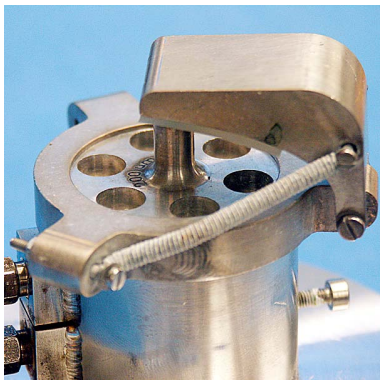

Figure 21: (a) The redesigned nozzle with mounting holes and a 100 μm hole. (b) The nozzle cap in place and closed over the nozzle.

Three different sizes of nozzle were prepared: 200 μm, 100 μm, and 50 μm. The 50 μm nozzle was easily clogged by particulates in the system and ultimately only the 200 μm and 100 μm nozzles were used for testing.

6.1.3 Voice Coil and Piston Assembly

The same voice coil was used in the handheld device (BEI Kimco model LA25-42-000A). The piston assembly was also similar to the benchtop proof-of-concept, except that the force sensor was removed from the system and replaced with an axial misalignment coupling to prevent the system from being overconstrained. Also, instead of using a 3 mm shaft as the piston, a piston from a Hamilton [7] syringe (model 5495-30, 1750.5TLLX 250 uL Syringe W/STP) was used to improve the seal inside the drug cylinder (Figure 22).

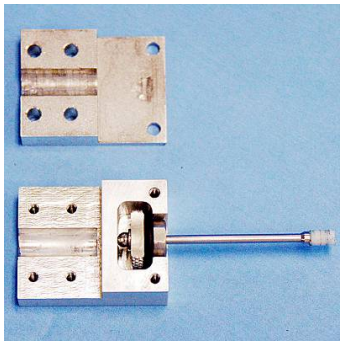

Figure 22: The misalignment coupling with the Hamilton syringe piston.

6.1.4 Auto-loading System

Automatically loading the device with fluid would reduce errors and increase its throughput. Therefore, an auto-loading system was designed by Brian Hemond. By attaching a 50 mL test

tube with screw-on cap to the refill port and selectively pressurizing the test tube with argon, the device could be refilled automatically by the software after each injection.

6.1.5 Sensors

The position and pressure sensors were the same ones used in the benchtop proof-of-concept. The force sensor was not included in the handheld prototype.

6.1.6 Electronics and Software

The electronics and software were similar to the benchtop proof-of-concept, with only minor revisions and updates to the software as needed to improve functionality or add safety checks so the device could not be fired until it had been filled with fluid.

6.2 Device Characterization

The handheld prototype was tested after its completion to make sure that it performed as expected.

6.2.1 Repeatability

Repeatability of the device was tested with the 100 μm and 200 μm nozzles. The results (Figure 23) show that the device fires repeatably with either nozzle. The red "error" bar of the graph indicates the difference between the amount of fluid measured that exited the nozzle and the theoretical amount of fluid that should have exited based on the travel of the piston (measured by the position sensor). Differences in the theoretical and actual volumes could be caused by air in the system, small losses of fluid out the bleed port or through the check valve, errors in the position sensor measurement, a drop of fluid left on the device nozzle, or other factors.

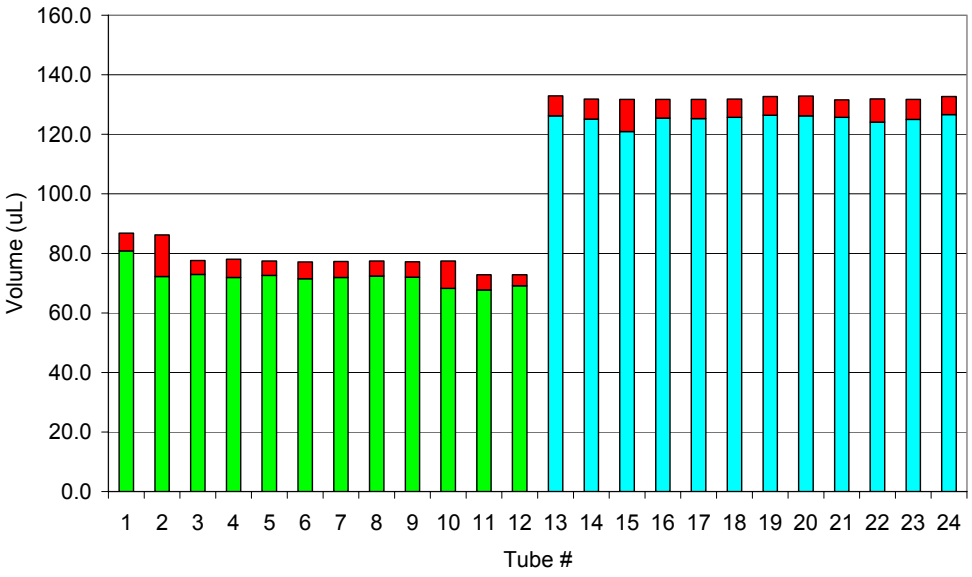

Figure 23: Repeatability of volume of fluid ejected from the handheld prototype device. The green bars correspond to the 100 μm nozzle and the blue bars correspond to the 200 μm nozzle. The red bars indicate the difference between the theoretical volume ejected based on the position sensor and the measured volume ejected.

This device shows much better repeatability than the proof-of-concept device (standard deviation is 3.3 µL for the 100 µm nozzle and 1.5 µL for the 200 µm nozzle). Therefore, the amount of fluid injected into samples would be much more consistent, yielding better scientific results.

6.2.2 In Vitro Dye Injections

Injections of Bromocresol Green dye solution using the handheld prototype gave similar results to those from the benchtop device experiments. By varying the jet power profile, the depth of injection below the epidermis could be varied. Also, it appeared that the most important parameter in determining the depth of injection was the peak jet power, as shown in Figure 24. By increasing the peak jet power, the depth of the injection increased dramatically.

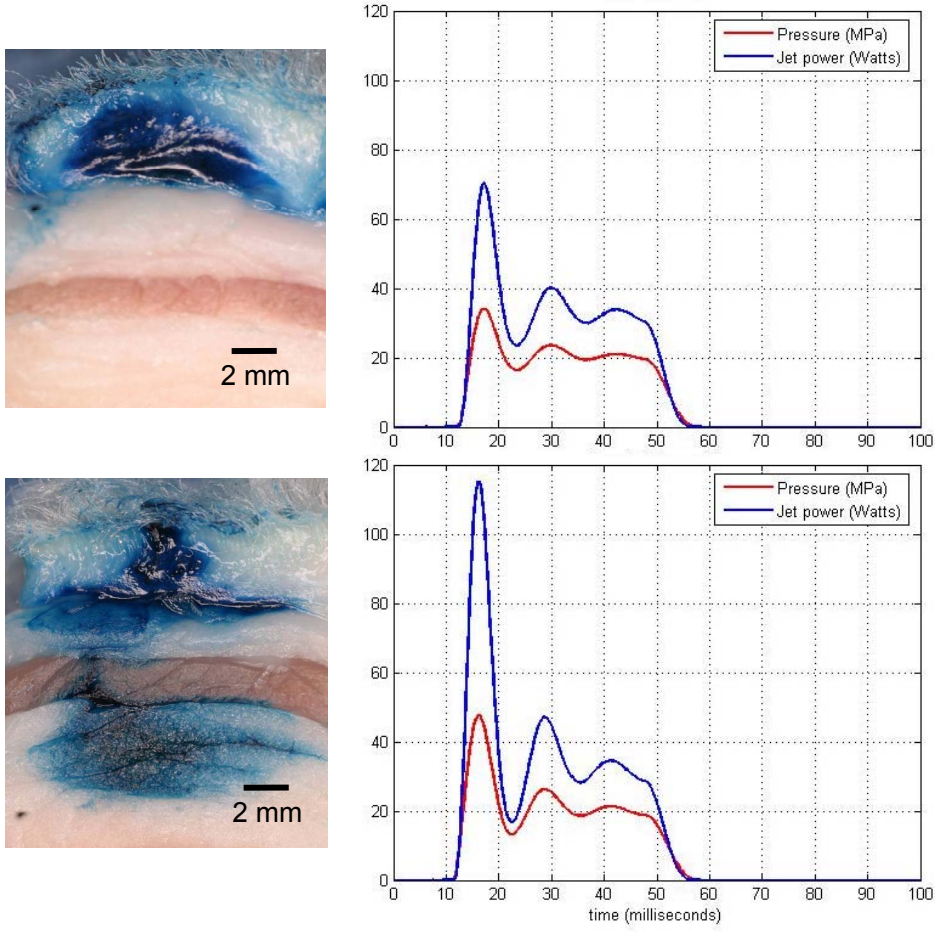

Figure 24: Depth of injection increases as peak jet power increases.

The controllability of the device provided an opportunity to develop voltage waveforms precisely for each depth of injection need. Also, the waveforms would need to be different for each nozzle diameter if it was indeed the jet power that indicates the depth of the injection (as theorized in Section 4.2). Therefore, many different voltage waveforms were created and tested on tissue all using the same handheld device. We focused on waveforms that delivered liquid to the dermis, since this is the optimal location for collagenase delivery. A summary of results for the 100 µm and 200 µm nozzle waveforms is shown in Figure 25. Several quantitative parameters were

calculated by an imaging program written by Andrea Bruno in Matlab [21] (see Appendix C) and the averages are presented in the figure as well. Some waveforms appear to produce more uniform injections, which is desirable. Also, the average depth of injection is important, which is quantified by the two Mean Depth measurements.

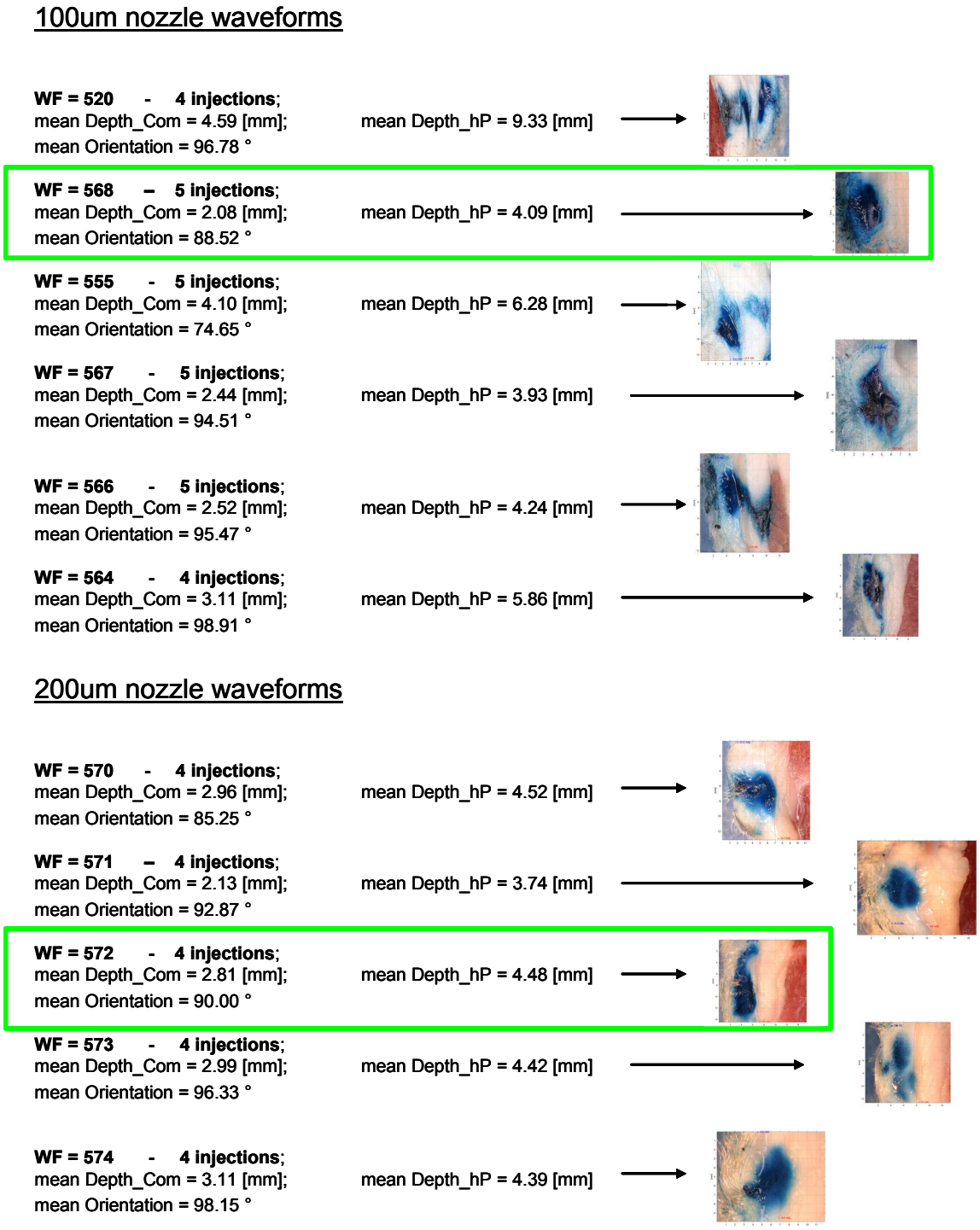

Figure 25: Injection results for different waveforms created for the 100 µm and 200 µm nozzles with the goal of injecting fluid into the dermis. The selected waveforms used for in-vivo experimentation are circled in green. (Figure courtesy of Andrea Bruno).

6.2.3 In Vitro Activity Testing

In vitro activity testing with collagenase was performed the same way as the activity assays were performed with the benchtop device. The results were the same: the collagenase is still active after being injected into a test tube or into tissue from the handheld controllable NFI prototype.

6.2.4 In Vivo Activity Testing

After repeatability testing, in-vitro injection depth testing, and in-vitro activity testing, the next step was to test the handheld device on a live sheep. A 10 week old Suffolk-cross wether was chosen as the test subject. The collagenase mixture from the activity testing was injected into the midside of the animal and the response was monitored for several weeks. Controls consisted of 1xRB buffer injected via the NFI, 1xRB buffer injected by a conventional 27.5 gauge needle (190.5 µm diameter), and collagenase injection by a 27.5 gauge needle. The outline of the test locations is shown in Figure 26.

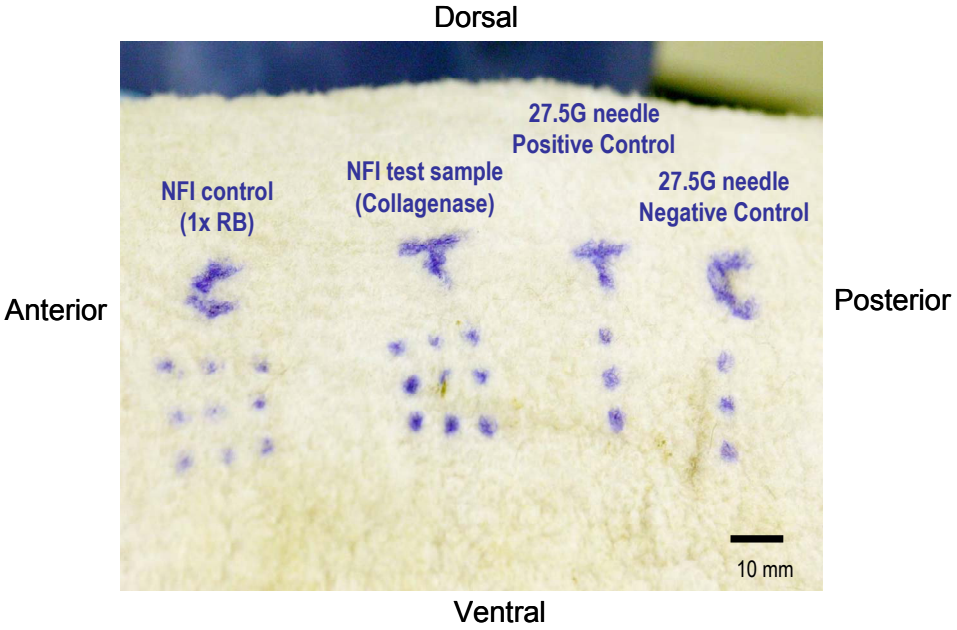

Figure 26: Location of test injections on the midside of a 10-week old Suffolk-cross wether.

The lamb was sedated while the injections were performed. The injections with the prototype device were performed by Dawn Wendell and the needle injections were performed by Dr. Cathy Hogan (Figure 27). The intended depth of the injection was into the dermis, about 2 to 4mm deep in the tissue.

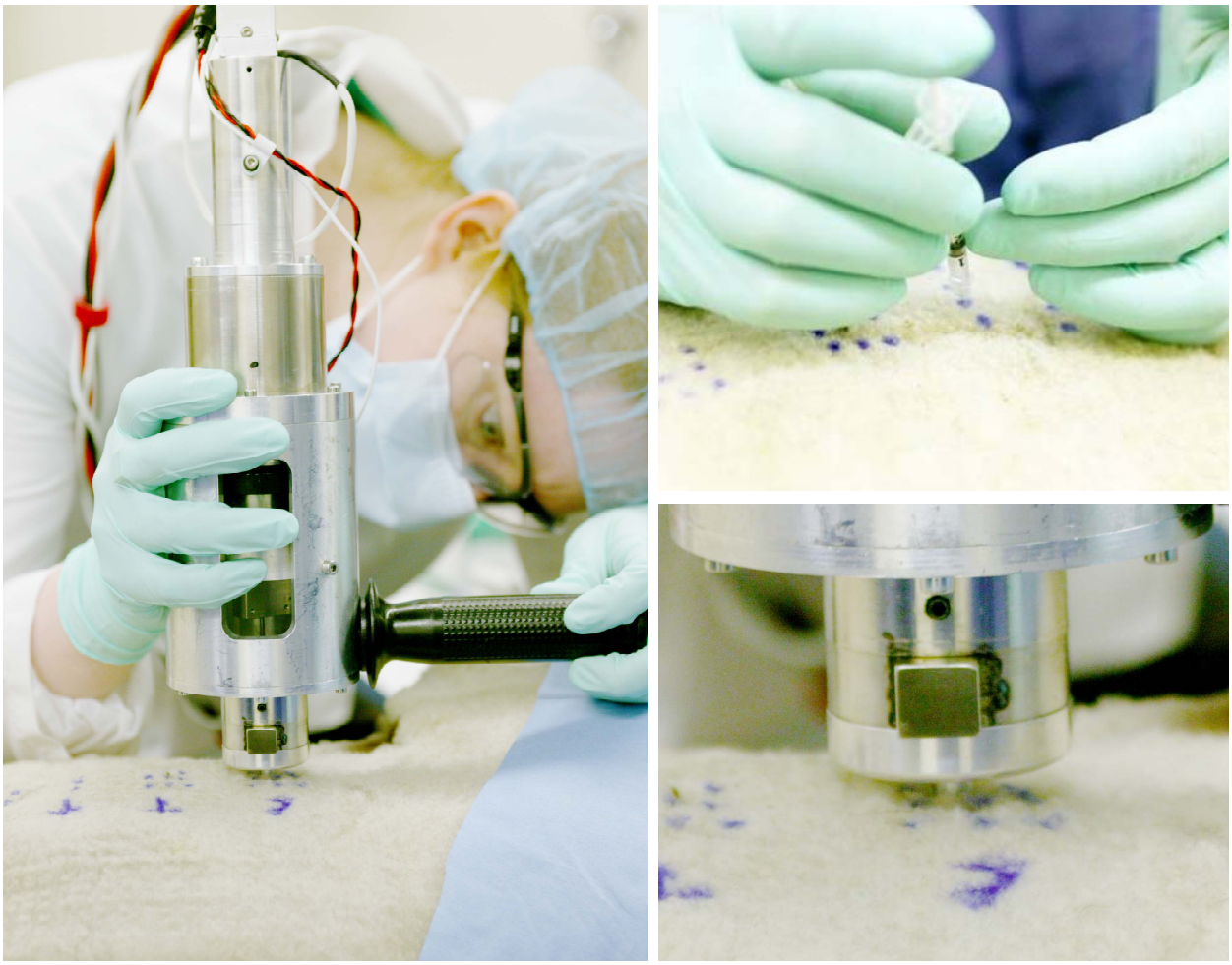

Figure 27: (a) Dawn Wendell uses the handheld NFI prototype. (b) Dr. Cathy Hogan injects with conventional 27.5 gauge syringe. (c) Closeup of the nozzle of the NFI prototype; the nozzle is penetrating the wool layer.

During the injections, a small amount of blood appeared at two of the NFI injection sites. Otherwise, there was no noticeable difference between the needle injections and the NFI injections. The lamb was monitored for more than 6 weeks after the injections.

6.2.5 Summary of Results

Over the course of 6 weeks of monitoring the lamb, photographs were taken of each of the injection sites. A summary of the results is shown in Figure 28. At Day 9 post-injection, the injection sites were shaved so that Dr. Hogan could acquire biopsies to check for cellular evidence of collagenase activity. Visually, it was clear from the results of the experiment that the 1xRB buffer had no effect whether it was injected by the NFI or by a needle, and that collagenase caused similar hair loss and scarring whether it was injected by the NFI or a needle (Figure 28).

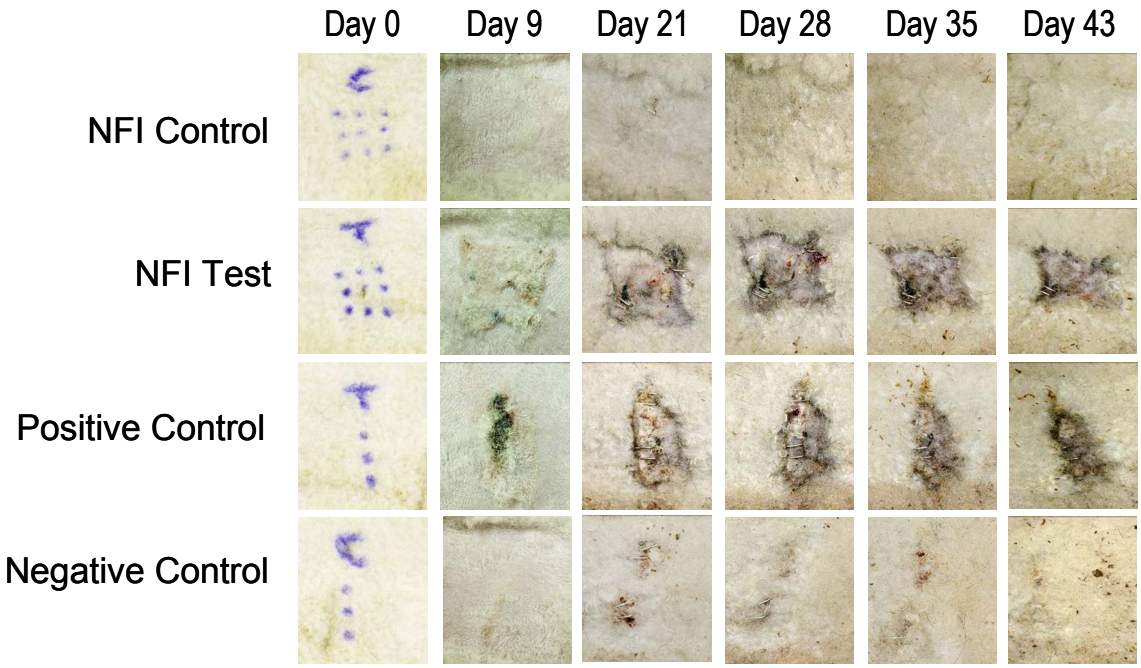

Figure 28: Results of injections of 1xRB buffer and collagenase into lamb midside using NFI and conventional needle injections. In the figure, NFI Control refers to injections of buffer via the NFI, NFI Test refers to injections of collagenase via the NFI, Positive Control refers to needle injections of the collagenase, and Negative Control refers to needle injections of the buffer. (Figure courtesy of Dr. Hogan).

The biopsy plugs that were taken on Day 9 were trimmed and prepared for paraffin embedding by Dr. Hogan. The samples were then sent to the MIT Histology Lab where they were embedded, sectioned, and stained with Masson's Trichrome (which stains collagen blue). Photomicrographs of the samples can be seen in Figure 29.

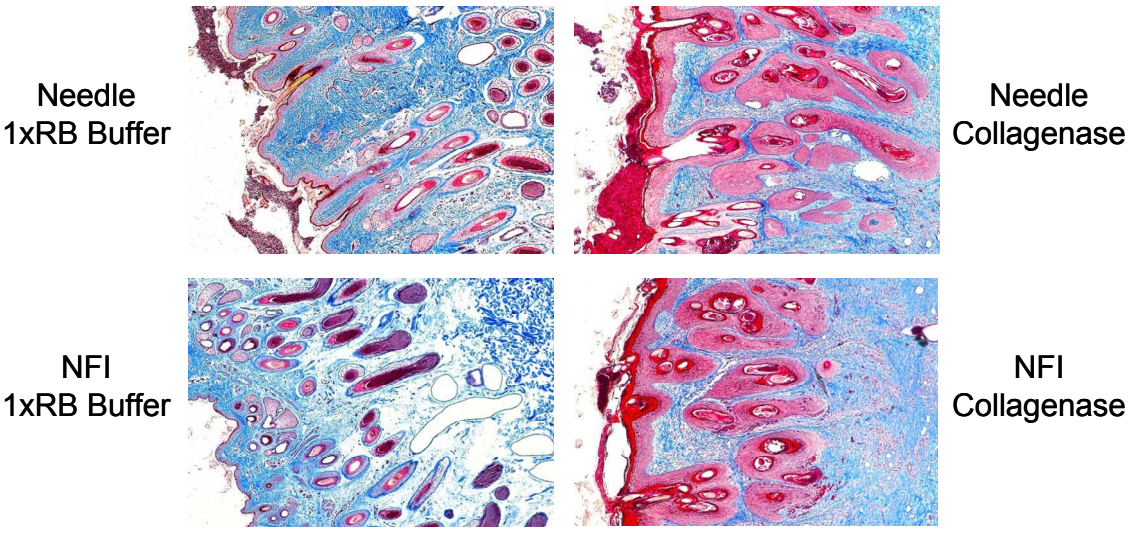

Figure 29: Photomicrographs of tissue sections stained with Masson's Trichrome, 9 days post-injection. Both samples injected with buffer look similar to each other and similar to healthy tissue. Both samples injected with collagenase look similar to each other and significantly different than normal tissue. The collagenase-injected tissue samples show changes in tissue morphology including a thickened epidermis, distruption of hair follicles, and proliferation of collagen. (Images courtesy of Dr. Hogan).

The samples injected with buffer both appear normal, but the samples injected with collagenase show changes in tissue morphology: thickened epidermis, disrupted hair follicles, and a proliferation of collagen. The proliferation of collagen is a typical wound response to injection with collagenase.

These in-vivo experiments prove that collagenase is still active after injection with the handheld NFI device, and that NFI injection of collagenase is comparable to needle injection in sheep midside.

7 Conclusions and Future Directions

A handheld controllable needle-free injection device was designed and manufactured using a voice coil as the controllable actuator. The device was capable of injections of different depths into tissue based on the driving voltage waveform given to the voice coil. Collagenase injected by the device was still active post-injection in sheep tissue in-vitro and in-vivo. Also, collagenase delivered by the controllable NFI device resulted in the same pharmacological results as collagenase delivered by a 27.5 gauge needle.

The future work that would most benefit the controllable NFI project would be to create a tissue model that would allow the correlation of jet power with depth of injection. This model would probably vary based on the animal species, age, and perhaps even breed. However, this understanding would allow the user of a controllable NFI in the field to "dial in" the depth of the injection necessary and then have the controllable actuator deliver an injection with the appropriate jet power to produce that depth. This also has implications for a human market for this device. By adjusting the depth of injection, it could be possible to minimize pain and deliver drug to the correct depth every time, unlike a needle where medical errors can result in incorrect injections. Future work in this area could drastically improve healthcare for animals and humans alike.

Bibliography

[1] Centers for Disease Control, Atlanta, Georgia, USA. www.cdc.gov

[2] AE Techron, Inc., Elkhart, Indiana, USA. www.aetechron.com

[3] ANSYS Inc., Canonsburg, Pennsylvania, USA. www.ansys.com

[4] A. B. Baker and J. E. Sanders, "Fluid Mechanics Analysis of a Spring-Loaded Jet Injector," *IEEE Transactions on Biomedical Engineering*, vol. 26:2, pp. 235-242, 1999.

[5] BEI Technologies, Inc., Kimco Magnetics Division. Vista, California, USA. www.beikimco.com

[6] Bioject Medical Technologies, Incoporated. Tualatin, Oregon, USA. www.bioject.com

[7] Centers for Disease Control, "Hepatitis B associated with jet gun injection—California," *Morbidity and Mortality Weekly Report*, vol. 23, pp. 373-376, June 13, 1986.

[8] Futek Advanced Sensor Technology. Irvine, California, USA. www.futek.com

[9] Hamilton Company. Reno, Nevada, USA. www.hamiltoncomp.com

[10] Hemond, Brian. "A Lorentz-force Actuated Controllable Needle-free Drug Delivery System," *Massachusetts Institute of Technology*. Cambridge, Massachusetts, February 2006.

[11] R. A. Hingson and J. G. Hughes, "Clinical studies with jet injection: A new method of drug administration," *Anesth. Analg. Cleve.*, vol. 26, pp. 221-230, 1947.

[12] Howard-Jones, "A Critical Study of the Origins and Early Development of Hypodermic Medication," *Journal of the History of Medicine and Allied Sciences*, vol 2, pp. 201-249, 1947.

[13] Kistler Instruments, Winterthur, Switzerland. www.kistler.com

[14] S. Landau, U.S. Patent Application 20 020 123 717, September 5, 2002.

[15] S. Landau, U.S. Patent Application 20 020 123 718, September 5, 2002.

[16] S. Landau, R. B. Hubler, J. M. Stiggelbout, U.S. Patent Application 20 050 075 601, April 7, 2005.

[17] S. Landau, C. Sautter, U.S. Patent Application 20 050 119 608, June 2, 2005.

[18] S. Landau, D. E. Williamson, U.S. Patent Application 20 040 111 054, June 10, 2004.

[19] S. Landau, D. Williamson, J. R. Marshall, U.S. Patent Application 20 030 225 368, December 4, 2003.

[20] S. Landau, D. E. Williamson, J. R. Marshall, U.S. Patent Application 20 040 199 106, October 7, 2004.

[21] LINOS Photonics, Inc. Milford, Massachusetts, USA. www.linos-photonics.com/catalog/en/produkte/mechmakro.html

[22] The MathWorks. Natick, Massachusetts, USA. www.mathworks.com.

[23] A. Neracher, U.S. Patent Application 20 050 154 347, July 14, 2005.

[24] S. F. Peterson, C. N. McKinnon, Jr., P. E. Smith, T. Nakagawa, V. L. Bartholomew, U.S. Patent 5 520 639, May 28, 1996.

[25] J. Schramm-Baxter, J. Katrencik, S. Mitragotri, "Jet injection into polyacrylamide gels: investigation of jet injection mechanics," *Journal of Biomechanics*, vol. 37, pp. 1181-1188, 2004.

[26] J. Schramm and S. Mitragotri, "Transdermal Drug Delivery by Jet Injectors: Energetics of Jet Formation and Penetration," *Pharmaceutical Research*, vol. 19:11, pp. 1673-1697, 2002.

[27] J. Schramm-Baxter and S. Mitragotri, "Needle-free jet injections: dependence of jet penetration and dispersion in the skin on jet power," *Journal of Controlled Release*, vol. 97, pp. 527-535, 2004.

[28] J. Schramm-Baxter and S. Mitragotri, "Investigations of Needle-free Jet Injections," *Proceedings of the 26th Annual Conference of the IEEE EMBS*, pp. 3543-3546, 2004.

[29] Sentech, Inc., North Hills, Pennsylvania, USA. www.sentechlvdt.com

[30] G. J. Sibert, P. J. Dominowski, J. C. Frantz, U.S. Patent Application 20 040 158 195, August 12, 2004.

[31] Vision Research, Inc. Wayne, New Jersey, USA. www.visiblesolutions.com

[32] Yamazaki Mazak Corporation, Oguchi, Japan. www.mazak.com

Appendix A: Selected Device Drawings

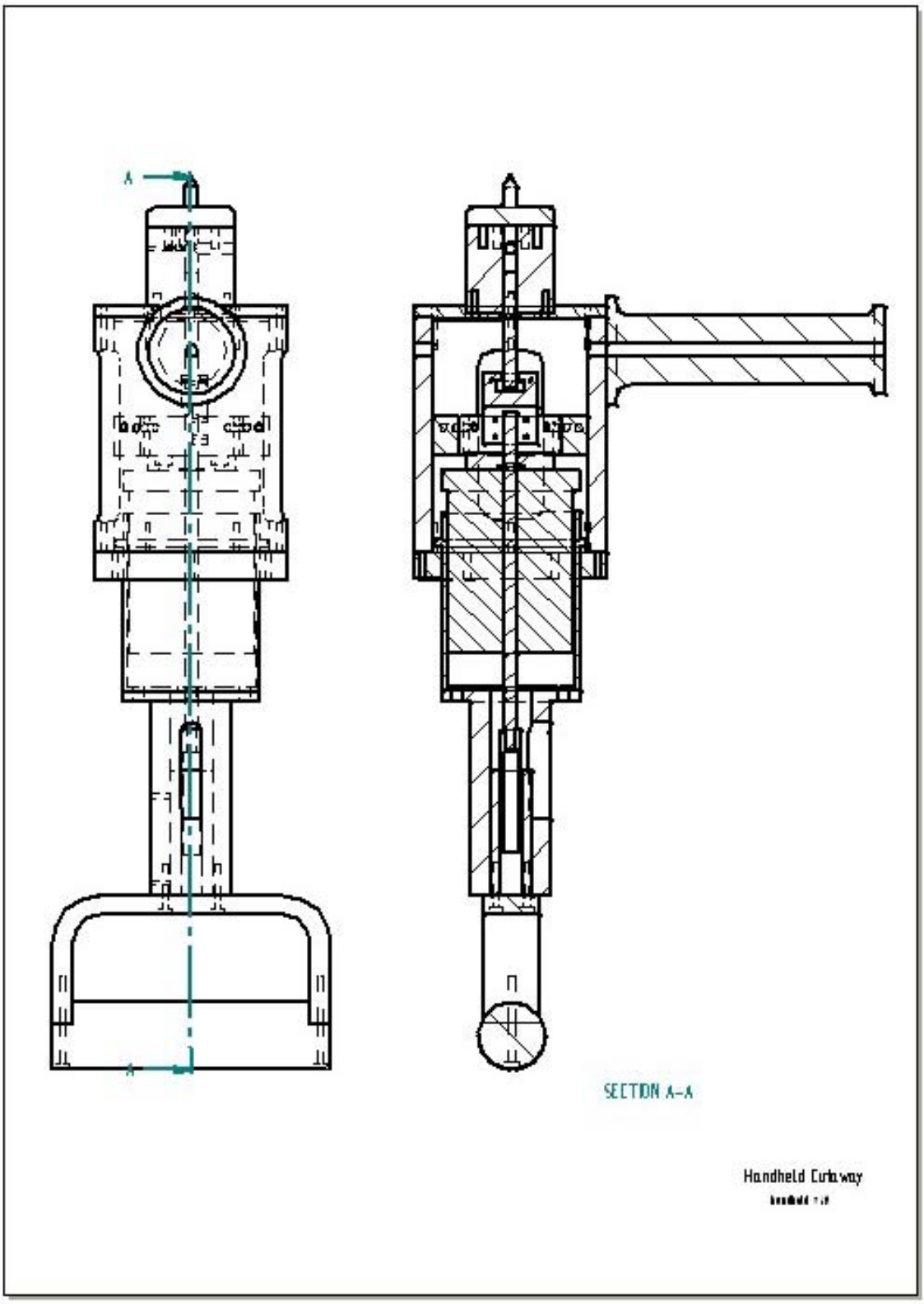

Appendix B: Matlab Script for Jet Power Calculation

```
clear;

%*****************************************
%
% NW Abbey Needless Injection Analysis
%              March 15 2005
%          Single File Analysis
%    (edited for new software channels)
%  modified to calculate volume ejected based on initial and final piston
%   position 8-15-05
%  added jet power and jet velocity to the graphs  9-19-05
%*****************************************


%Change directory to where data is
%cd 'C:\Documents and Settings\Dawn M. Wendell\Desktop\injector
software\bin\Debug';

%Choose file to be analyzed
first = input('Enter the first file number you wish to analyze: ','s');
last = input('Enter the last file number you wish to analyze: ','s');
noz = input('Nozzle? (enter 1 for 100um, 2 for 200um): ');

colors = ['r  '; 'g  '; 'b  '; 'm  '; 'k  '; 'y  '; 'c  '; 'r--'; 'g--'; 'b--
'; 'm--'; 'k--'; 'y--'; 'c--'; 'r-.'; 'g-.'; 'b-.'; 'm-.'; 'k-.'; 'y-.'; 'c-
.'; 'r  '; 'g  '; 'b  '; 'm  '; 'k  '; 'y  '; 'c  '; 'r--'; 'g--'; 'b--'; 'm-
-'; 'k--'; 'y--'; 'c--'; 'r-.'; 'g-.'; 'b-.'; 'm-.'; 'k-.'; 'y-.'; 'c-.'];

datanums = str2num(first):str2num(last);

for j=str2num(first):str2num(last);
file = strcat('data',num2str(j),'.csv');
color = colors(j-str2num(first)+1,:);

%Load Files
    data = csvread(file,8,1);

%Split Data
    pressure = data(:,9)*11;
    position = (data(:,8))*2; % - data(1,10));
    position = position-min(position);
   % voltage = data(:,10)*2;
   % current = data(:,11);
   % drive = data(:,12)*10;
    time = data(:,1);
    t = time;
    %velocity = (position(2:length(position))-position(1:length(position)-
1))/(time(2)-time(1));
    %velocity = velocity*5;  %fixes units

    pos1 = position/2;
    A_bore = 3.1415/4*(0.1285*25.4)^2;  %mm^2
    V_swept = A_bore*(pos1(end)-pos1(1));
```

```
    A_noz = 3.1415/4*((noz*0.1)^2);  %mm^2
    %velocity = velocity*(A_bore/A_noz)/100;

%Integrated Bernoulli
    volume = 0;
    vel = sqrt(2000*pressure);
    for i=1:length(pressure);
    volume = volume + (0.1*A_noz*vel(i));
    vol(i) = volume;
    end;
    volume;

%Jet Power
    rho=1000;    %water
    Po=0.5*rho*(A_noz/1000000)*vel.^3;    %all in standard units (m, sec)
    maxPo = max(Po);

%Plot Data
    figure(1);

    subplot(5,1,1)
    HP = plot(t,pressure,color);
    xlim([0 100])
    ylim([0 75])
    set(HP, 'LineWidth',1)
    ylabel('Pressure (MPa)')
    hold on
    grid on

    subplot(5,1,4)
    HC = plot(t,vel,color);
    set(HC, 'LineWidth',1)
    ylabel('Jet Velocity (m/s)')
    hold on
    grid on

    subplot(5,1,2)
    HD = plot(t,position,color);
    set(HD, 'LineWidth',1)
    ylabel('Position (mm)')
    hold on
    grid on

    subplot(5,1,3)
    HD = (plot(t,vol,color));
    set(HD, 'LineWidth',1)
    ylabel('volume ejected (uL)')
    hold on
    grid on

    subplot(5,1,5)
    HD = (plot(t,Po,color));
    set(HD, 'LineWidth',1)
    xlabel('time (msec)')
    ylabel('Jet Power (Watts)')
    hold on
    grid on
```

```
    subplot(5,1,1)
    title('Injection Results')
    datnums = transpose(datanums);
    legend(num2str(datnums))

    figure(2);
    HP = plot(t,pressure,color);
    ylim([0 70])
    set(HP, 'LineWidth',1)
    ylabel('Pressure (MPa)')
    xlabel('Time (ms)')
    hold on
    grid on
    title('Injection Pressures')
    datnums = transpose(datanums);
    legend(num2str(datnums))
end

    %text(32.5,27.5,strcat('Swept Volume = ',num2str(V_swept)))
%     [AX,H1,H2] = plotyy(t, voltage, t, position);
%     set(H1, 'LineWidth', 2);
%     set(H2, 'LineWidth', 2);
%     set(get(AX(2),'Ylabel'),'String','Position (mm)')
%     set(AX(1),'YLim', [0 170])
%     set(AX(1), 'XLim',[0 60])
%     set(AX(1),'YTick', 0:10: max(voltage))
%     set(AX(2),'YLim', [0 2*mean(position)])
%     set(AX(2),'YTick', 0:1: 2*mean(position))
   % axis([0 100 0 70]);
   % legend('pressure in MPa', 'current in amps', 'drive x 10', 'voltage in
volts', 'position in mm x2', 'velocity m/s /10', 'calc vol ejected/2
(uL)','Jet power (Watts)')

   % title(strcat('Results for  ',x))
```

Appendix C: Matlab Script for Quantitative Tissue Comparison (by Andrea Bruno, printed with permission)

```
%% Introduction;
%The user's intervention is really limited:
%Mainly she needs to crop the image to avoid tracking dye that is not in
%the tissue, draw the approximative lines of separation between epidermis
%and dermis and between dermis and subcutaneus fat. Then she needs to
%choose the ROIs (regions of interest) to further keep the algorithm to
%apply to wrong zones (dyed hair or scene background)

% set directory default;
clear;
pathname = 'C:\Documents and Settings\andrea\My
Documents\Work\injectionCampaign_june3';
close all
try
    load data.mat
    catch
end

index =[];
try
    index = data(end).Index;
catch
end

if isempty(index);
    index = 1;
else
    index = index + 1;
end

 %% image load
pathname = 'C:\Documents and Settings\andrea\My
Documents\Work\injectionCampaign_june3';
cd(pathname);
[filename, pathname] = uigetfile(  { '*.jpg',  'Jpeg file (*.jpg)'; ...
   '*.bmp','Bitmap file(*.bmp)'; ...
   '*.tif','Tif file (*.tif)';}, ...
   'Pick an image');
insertmass(filename);
I = imread([pathname,filename]);
imshow(I)


%% crop image step
% It allows to limit the size of the processed image in order to speed up
% the algorithm
Ic = imcrop(I);
imshow(Ic)
Ic = im2double(Ic);
```

```
%% image processing step
% The algorithm works in an RGB workspace. After filtering, to smooth the
% image and ease the thresholding, the Blue dye is tracked subtructing the
% Red and Green channels to the Blu one. The algorithm uses also
% morphological reconstruction to fill eventual holes.

  filt = fspecial('disk',6);
  If = imadjust(Ic,stretchlim(Ic),[0 1]);
  If = imfilter(If,filt);

 imshow(If), title('Draw approximative epidermis line')
 xy_epidermis_est = gpointspline;
 title('Draw approximative fat tissue line')
 xy_tissue_est = gpointspline;

 %  xy_2 = gpointspline;
%  xy_3 = gpointspline;
%  xy_4 = gpointspline;

R=Ic(:,:,1);
G=Ic(:,:,2);
B=Ic(:,:,3);
[m,n]=size(R);

y1 = B - R;
y2 = B - G;

%y1 = imadjust(y1,stretchlim(y1),[0 1]);

y2 = imadjust(y2,stretchlim(y2),[0 1]);
y2 = imfill(y2, 'holes');

imshow(y2),title('Intensity rapresentation of the tracked dye');

%%subplot(211),imshow(y2),title('B-G');
%subplot(212),imshow(y1),title('B-R');

%% BW conversion.
% A black and white conversion is accomplished to easily extract
% morphological parameters useful to characterized the injection.

% g = round(ginput(1))
% v = y2(g(2),g(1))

%filt = fspecial('disk',7);
%imshow(If), hold on,

%Two thresholds are chosen in order to track the diffusion of the dye into
%the tissue. This is done looking at the intensity values of the subtracted
%channels. The Higher is the intensity, the more concentrated is the dye.

[C,h] = contour(imfilter(y2,filt),5); axis ij;
set(h,'ShowText','on','TextStep',get(h,'LevelStep')*2)
```

```
BW = im2bw(y2,0.33);
imshow(BW), title('select ROI - Low Intensity')
BBB = roipoly;
BWL = BBB.*BW;

BW = im2bw(y2,0.83);
imshow(BW), title('ROI - High Intensity')
BBBL = roipoly;
BWH = BBBL.*BW;

subplot(211), imshow(BWL),title('select ROI - Low Intensity');
subplot(212), imshow(BWH),title('ROI - High Intensity');

%% Regions analysis
% The algorithm then measures a set of properties for
% each ROI. Someone of these, like the Area, are calculated working directly
on the
% BW images. Other, as center of mass, are calculated using the Intensity
% image.

h = regionprops(double(BWH),'Area',
'Centroid','Orientation','Solidity','Extrema');

%imshow(y2), title('Injected stuff')

l = regionprops(double(BWL),'Area', 'Centroid','Extrema','Orientation');

centroids = centroid(y2.*BBB);
centroidsl = centroid(y2.*BBBL);

 el_sx = l.Extrema(7:8,:);
el_dx = l.Extrema(3:4,:);

[lsx,pos] = min(el_sx(:,1));
lPsx = [lsx,el_sx(pos,2)];     %%% Left extreme point

[ldx,pos] = max(el_dx(:,1));
lPdx = [ldx,el_dx(pos,2)];     %%% Right extreme point

eh_sx = h.Extrema(7:8,:);
eh_dx = h.Extrema(3:4,:);

[hsx,pos] = min(eh_sx(:,1));
hPsx = [hsx,eh_sx(pos,2)];     %%% Left extreme point

[hdx,pos] = max(eh_dx(:,1));
hPdx = [hdx,eh_dx(pos,2)];     %%% Right extreme point

[position_HighDens,side] = grelpos(xy_tissue_est,
xy_epidermis_est,hPsx,hPdx);
[position_LowDens,side] = grelpos(xy_tissue_est, xy_epidermis_est,lPsx,lPdx);

res =      0.0147; %fastcal;
```

```
%% Visual proof
% Of course, image are saved to allow the operator to check and determine
% the qualitity of the injection using her qualitative assessment as well
% as the quantitative parameters.
figure1 = figure('Color',[1 1 1]);

axes1 = axes(...
  'Layer','top',...
  'TickDir','out',...
  'YDir','reverse',...
  'Parent',figure1);
[m,n] = size(Ic(:,:,1));
x = [1:n]*res;
y = [1:m]*res;

imshow(Ic,'XData',x,'YData',y)
axis on, grid on,
hold on

ylabel('[mm]');

if side == 1   %epidermis at the right side
plot(hPsx(1)*res,hPsx(2)*res,'+','Color',[0,1,0])
plot(lPsx(1)*res,lPsx(2)*res,'o','Color',[0,1,0])
else
plot(hPdx(1)*res,hPdx(2)*res,'+','Color',[0,1,0])
plot(lPdx(1)*res,lPdx(2)*res,'o','Color',[0,1,0])
end
plot(xy_epidermis_est(1,:)*res,xy_epidermis_est(2,:)*res,'b--');
text(xy_epidermis_est(1,1)*res,xy_epidermis_est(2,1)*res,'\leftarrow E-D
ABL',...
     'HorizontalAlignment','left','Color','b')
plot(xy_tissue_est(1,:)*res,xy_tissue_est(2,:)*res,'r--');
text(xy_tissue_est(1,end)*res,xy_tissue_est(2,end)*res,'\leftarrow D-F
ABL',...
     'HorizontalAlignment','left','Color','R')
% plot(centroids(:,1), centroids(:,2), 'b*')
% plot(centroidsl(:,1), centroidsl(:,2), '+')

resp = DYLP;

if resp == 'No!'

    title('Pick: 1. point lP  - 2. point hp');
    lP = ginput(1)/res;
    hP = ginput(1)/res;
    close;
    imshow(Ic,'XData',x,'YData',y)
    axis on, grid on,
    hold on
    plot(hP(1)*res,hP(2)*res,'+','Color',[0,1,0])
    plot(lP(1)*res,lP(2)*res,'o','Color',[0,1,0])

    plot(xy_epidermis_est(1,:)*res,xy_epidermis_est(2,:)*res,'b--');
```

```
    text(xy_epidermis_est(1,1)*res,xy_epidermis_est(2,1)*res,'\leftarrow E-D
ABL',...
        'HorizontalAlignment','left','Color','b')
    plot(xy_tissue_est(1,:)*res,xy_tissue_est(2,:)*res,'r--');
    text(xy_tissue_est(1,end)*res,xy_tissue_est(2,end)*res,'\leftarrow D-F
ABL',...
        'HorizontalAlignment','left','Color','R')

    [val_lP, pos1] = distance(If,lP,xy_epidermis_est);
    [val_hP, pos2] = distance(If,hP,xy_epidermis_est);
    [tiss_lP, der_pos1] = distance(If,lP,xy_tissue_est);
    [tiss_hP, der_pos2] = distance(If,hP,xy_tissue_est);,'Color',[0,1,0]

else
    if side == 1
        [val_lP, pos1] = distance(If,lPsx,xy_epidermis_est);
        [val_hP, pos2] = distance(If,hPsx,xy_epidermis_est);
        [tiss_lP, der_pos1] = distance(If,lPsx,xy_tissue_est);
        [tiss_hP, der_pos2] = distance(If,hPsx,xy_tissue_est);
    else
        [val_lP, pos1] = distance(If,lPdx,xy_epidermis_est);
        [val_hP, pos2] = distance(If,hPdx,xy_epidermis_est);
        [tiss_lP, tiss_pos1] = distance(If,lPdx,xy_tissue_est);
        [tiss_hP, tiss_pos2] = distance(If,hPdx,xy_tissue_est);
    end
end

[val, pos] = distance(If,centroids,xy_epidermis_est);

imname = filename(1:end-4);
for gg = 1:length(imname)
    if imname(gg) == '-'
        imname(gg) = '_';
    end
end

cd([pathname '\pics']);
eval(['saveas(gcf' ',' '''' imname 'ELAB.jpg' '''' ',' '''' 'jpeg' ''''
')']);

%% SAVE DATA
%  Quantitative parameters are saved into a database. This structure has
%  the following information:
% Name: Name of the processed image
% Depth_CoM: Distance between the approximative epidermis line and the
% center of mass of the high intensity ROI
% Area: Area of the High Intensity Zone
% Orientation: the angle between the x-axis and the major axis
% of the ellipse that has the same second-moments as the region
% Solidity:  the proportion of the pixels in the convex hull that are also
% in the region. Computed as Area/ConvexArea (ConvexArea is the area in the
convex hull,
% with all pixels within the hull filled in.
% Diffusion: Three component: [a b c]; a is the ratio Area High intesity on
Area
% Low intensity; b is magnitude of the differnce vectore between the center
```

```
%of mass of the High intensity region and Low intensity region;
%c is the direction of the previous vector;
% Depth_lP: greatest depth of the Low intensity zone (with respect to the
epidermis)
% Depth_hP: greatest depth of the High intensity zone (with respect to the
% epidermis)
% Depth_lP_subTiss: greatest depth of the Low intensity zone (with respect to
the sub fat tissue)
% Depth_hP_subTiss: greatest depth of the High intensity zone (with respect
to the
% sub fat tissue)

% PosLowDensity: reminder of the position of High intensity zone
% PosHighDensity:  reminder of the position of High intensity zone
% InjectedMass: Difference between mass before injection and after the
% injection (user's input)
% WaveForm: user's input
% Index: database index;

Dif = h.Area/l.Area;
vect = centroidsl(1)-centroids(1) + i*(centroids(2)-centroidsl(2));
magn = abs(vect)*res; %[mm]
ang = angle(vect);
ang = angle(vect)*180/3.14; %[degree]

%          imagesc(Ic); hold on,axis ij
%          plot(centroids(1),centroids(2),'+'),
%          plot(centroidsl(1),centroidsl(2),'o')

eval(['data(' num2str(index) ')' '= struct(' '''' 'Name' '''' ',' 'imname'
',' '''' 'Depth_CoM' '''' ','  'val*res' ',' '''' 'Area' '''' ','...
    'h.Area*res*res' ',' '''' 'Orientation' '''' ...
    ',' 'h.Orientation' ',' '''Solidity''' ',' 'h.Solidity' ',' ''''
'Diffusion' '''' ',' '[Dif,magn,ang]' ',' ...
    '''' 'Depth_lP_Derm' '''' ',' 'val_lP*res' ',' '''' 'Depth_hP_Derm' ''''
',' 'val_hP*res' ',' ...
    '''' 'Depth_lP_SubTiss' '''' ',' 'tiss_lP*res' ',' ''''
'Depth_hP_SubTiss' '''' ',' 'tiss_hP*res' ',' ...
    '''' 'PosLowDensity' '''' ',' 'position_LowDens' ',' ...
    '''' 'PosHighDensity' '''' ',' 'position_HighDens'  ',' ...
    '''' 'InjectedMass' '''' ',' 'mass' ',' ...
    '''' 'WaveForm' '''' ',' 'waveform' ',' '''' 'Index' '''' ',' 'index)']);

%% Clear
cd(pathname);
data(end)
if index == 1;
save data.mat data %-append
else
 save data.mat data -append
end
close all
clear all
load data.mat
```

```
%% Edge finding
% % create disk-shaped structure element
% se = strel('rectangle', [20,20]);
%
% % perform bottom hat filter
% Ibot = imbothat(P, se);
%
% % perform top hat filter
% Itop = imtophat(P, se);
%
% % subtract images to enhance contrast (lower right)
% Ienhance = imsubtract(imadd(Itop, P), Ibot);
%
% % convert objects of interest
% Iec = imcomplement(Ienhance);
%
% % detect imtensity valleys
% Iemin = imextendedmin(Iec, 2);
% imshow(Iemin)
% Iimpose = imimposemin(Iec, Iemin);
% imshow(Iimpose)
% % watershed segmentation
% wat = watershed(Iimpose);
% imshow(wat)
% % label separate regions
% rgb = label2rgb(wat);
% imshow(rgb)
%
% % extract features from label matrix
% stats = regionprops(wat, 'Area', 'Orientation');
% area = [stats(:).Area];
% orient = [stats(:).Orientation];
% figure('pos',[54 313 658 372])
% plot(area, orient, 'b*')
% title('Relationship of Particle Orientation to Area')
% xlabel('Area (pixels)'), ylabel('Orientation (deg)')
% shg, pause
%
% % asses shape by exploring aspect ratio of detected features
% stats = regionprops(wat,'MajorAxisLength','MinorAxisLength');
% figure, plot([stats.MajorAxisLength],[stats.MinorAxisLength],'.')
% xlabel('Major Axis Length (pixels)')
% ylabel('Minor Axis Length (pixels)')
%
%
% BW = edge(P,'prewit');
% imagesc(BW)
%
% % HSV workspace
%         If = imfilter(Ic,filt);
% %         If = imadjust(If,stretchlim(If));
% %
%         HSV = rgb2hsv(If);
%         imagesc(HSV)
%
% %         P = hsv2rgb(P);
```

```
% %         subplot(2,2,1), imagesc(HSV(:,:,1)); title('H')
% %         subplot(2,2,2), imagesc(HSV(:,:,2));title('S')
% %         subplot(2,2,3), imagesc(HSV(:,:,3));title('V')
% %         subplot(2,2,4), imagesc(P);
%
%         P = rgb2gray(P);
%         P = imfilter(P,filt);
%
% % YCBCR processing
%
%  YCBCR = rgb2ycbcr(P);
%
%
% %% Fuzzy clustering
% [n,m] = size(y1);
% [N,M] = meshgrid(1:n,1:m);
%
% R=Ic(:,:,1);
% G=Ic(:,:,2);
% B=Ic(:,:,3);
% [m,n]=size(R);
% indice=m*n;
% num=0;
% for a1=1:m
%     for an=1:n
%         data=R(a1,an);
%         data1=G(a1,an);
%         data2=B(a1,an);
%         num=num+1;
%         VR(num)=data;
%         VG(num)=data1;
%         VB(num)=data2;
%     end
% end
% VP=[VR;VG;VB];
% VPT=double(VP');
% [center,U,of]=fcm(VPT,7);
%
% ly1 = reshape(y1,m*n,1);
% ly2 = reshape(y1,m*n,1);
% lN =  reshape(N,m*n,1);
% lM =  reshape(M,m*n,1);
%
% fcmdata = cat(2,ly2,lN,lM);
% [center, U, obj_fcn] = fcm(fcmdata, 3);
%
%
```